**LA-UR-23-26372**
**Approved for public release; distribution is unlimited.**

**Title:** Spark Channel Dynamics of Electrostatic Discharges

**Author(s):** Rose, John William

**Intended for:** PhD thesis defense presentation at Colorado School of Mines (CSM).

**Issued:** 2023-07-14 (rev.1)

Los Alamos
NATIONAL LABORATORY

# Spark Channel Dynamics of Electrostatic Discharges

John W. Rose
Department of Physics, Colorado School of Mines
W-10, Los Alamos National Laboratory

June 15, 2023

# Introduction to ESD and modeling approaches

# Overview of electrostatic discharge (ESD) events

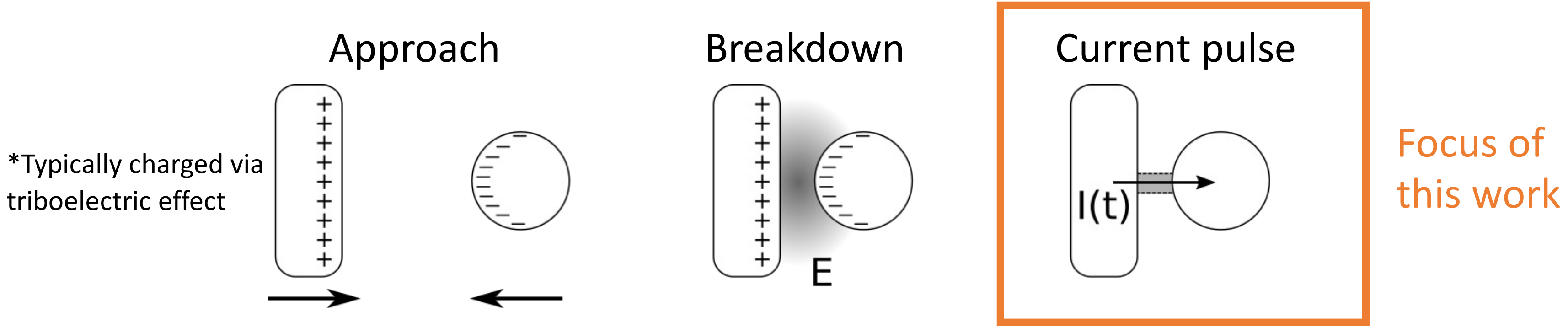


- Two-differently charged objects brought close together
- Resulting electric field $E$ strong enough to cause breakdown of air gap
- With sufficient stored charge, ionized gas filament (*spark channel*) forms
- Rapid transient current pulse $I = I(t)$ neutralizes charge difference
- Portion of stored energy goes toward resistive (Joule) heating of channel

# Categories of ESD hazard consequences

## Economic

- Semiconductor devices
  - Damage during assembly & handling
  - Industry implements controls to reduce loss fraction
  - Cost/benefit analysis for device production

RLC circuit model of ESD between conducting objects

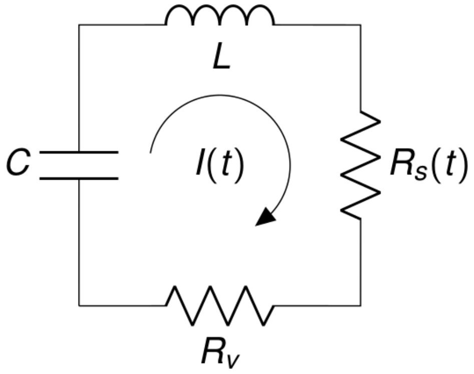


## Safety

Focus of this work

- Medical devices
  - Loss of function, subsequent injury or loss of life
- Flammable vapors and powders
  - Spark channel is ignition source for deflagration events
- Explosive/pyrotechnic devices
  - Unintended initiation of device

Initial stored energy:

$$\mathcal{E}_0 = \frac{1}{2} C \varphi_0^2$$

Energy dissipated in victim or current viewing resistor (CVR):

$$\mathcal{E}_v = R_v \int_0^t I^2(\tau) d\tau$$

# Modeling approaches for spark discharges

Used by this work

## Nonlinear resistance (lumped model)

- Based on limiting cases for spark channel energy balance
- Lowest computational cost (ODE only)
- No radial structure for thermal variables
  - Only indirect comparison to experiment (measured circuit variables)

## Hydrodynamic (thermal equilibrium)

- Mass, momentum, energy conservation in 1-D radial/2-D axisymmetric geometry
- Local Thermodynamic Equilibrium (LTE)
  - Common temperature $T$ for all species
  - Valid for fast electron-ion relaxation times
  - Equation of state (EOS) for air properties

## Kinetic (thermal non-equilibrium)

- Species populations found through rate equation system (highest comp. cost)
- Reaction rates (e.g. ionization) determined through cross sections
  - Data for air species *active research area*

## Two-temperature hydrodynamic

- Similar to LTE models, but electrons are out of equilibrium with ions and neutrals ("heavy species")
- Need to have EOS and transport properties for both $T_e$ and $T$

Not currently feasible

Possible future work

Los Alamos NATIONAL LABORATORY

# Geometrical assumptions for modeling spark channel

Photo by C. A. M. Schrama

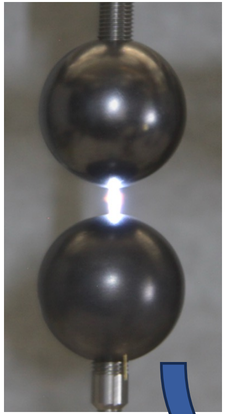

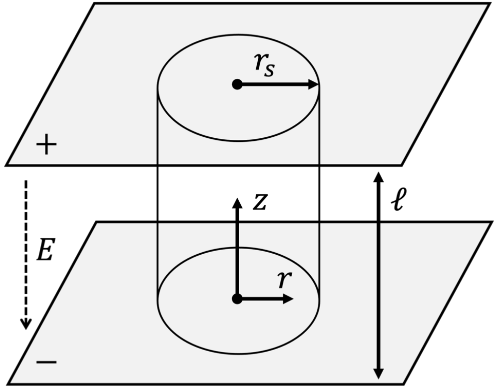


- Experimental imaging (CSM and others) shows spark channels for short gaps have high degrees of cylindrical symmetry
- Modeling assumes cylindrical symmetry is established during first nanoseconds and maintained up to a few microseconds

- Approximate gap near spark as having uniform electric field $E$
- Locally flat electrodes

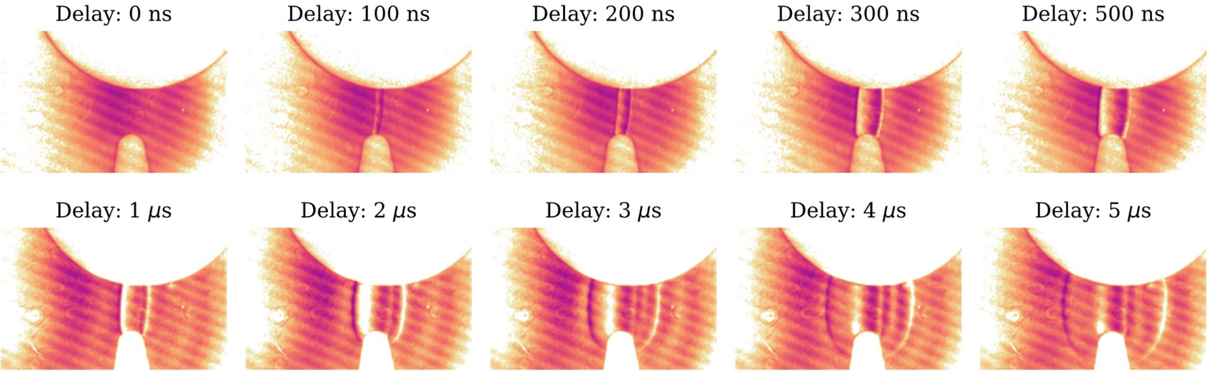


Schlieren images by C. A. M. Schrama

# Numerical scheme and verification

# Inviscid Euler equations with heat sources and thermal conduction (hydrodynamic conservation laws)

- For general coordinate systems,

$$\frac{\partial}{\partial t}\begin{pmatrix}\rho \\ \rho\vec{u} \\ \rho\varepsilon\end{pmatrix} + \nabla\cdot\begin{pmatrix}\rho\vec{u} \\ \rho\vec{u}\otimes\vec{u} \\ (\rho\varepsilon+p)\vec{u}+\vec{q}\end{pmatrix} = \begin{pmatrix}0 \\ -\nabla p \\ W_J + W_{\mathrm{rad}}\end{pmatrix}$$

- Specific total energy (J/kg) in terms of kinetic and specific internal energy $e$:

$$\varepsilon = e + \frac{1}{2}\vec{u}\cdot\vec{u} = e + \frac{1}{2}u^2$$

- Close with equation of state: $p = p(\rho, e), \quad T = T(\rho, e)$
- Heat conduction flux: $\vec{q} = -\kappa\nabla T$
- Joule heating term: $W_J = \vec{J}\cdot\vec{E} = \sigma E^2$
- Radiative transfer term $W_{\mathrm{rad}}$ discussed later

# Inviscid Euler equations with heat sources and thermal conduction (1-D symmetry)

- For 1-D symmetry ($\alpha = 0, 1, 2$ for planar, cylindrical, and spherical),

$$\frac{\partial}{\partial t}\begin{pmatrix}\rho \\ \rho u \\ \rho \varepsilon\end{pmatrix} + \frac{1}{r^\alpha}\frac{\partial}{\partial r}\begin{pmatrix} r^\alpha(\rho u) \\ r^\alpha(\rho u^2 + p) \\ r^\alpha\big((\rho\varepsilon + p)u + q\big)\end{pmatrix} = \begin{pmatrix} 0 \\ \frac{\alpha}{r}p \\ W_J + W_{\mathrm{rad}}\end{pmatrix}$$

- Specific total energy (J/kg) in terms of kinetic and specific internal energy $e$:

$$\varepsilon = e + \frac{1}{2}u^2$$

- Close with equation of state: $p = p(\rho, e), \quad T = T(\rho, e)$
- Heat conduction flux: $q = -\kappa \frac{\partial T}{\partial r}$
- Joule heating term: $W_J = \sigma E^2 = \sigma\left(\frac{I R_S}{\ell}\right)^2$

# Discretizing 1-D hydrodynamic equations

- Rewrite Euler equations in two forms suitable for finite volume method (FVM)

Non-conserving when discretized

- *Geometric source term* form,

$$\frac{\partial}{\partial t}\begin{pmatrix}\rho\\ \rho u\\ \rho\varepsilon\end{pmatrix}+\frac{\partial}{\partial r}\begin{pmatrix}\rho u\\ \rho u^2+p\\ (\rho\varepsilon+p)u+q\end{pmatrix}=-\frac{\alpha}{r}\begin{pmatrix}\rho u\\ \rho u^2\\ (\rho\varepsilon+p)u+q\end{pmatrix}+\begin{pmatrix}0\\ 0\\ W_J+W_{\mathrm{rad}}\end{pmatrix}$$

- *Geometric flux* form,

$$\frac{\partial}{\partial t}\begin{pmatrix}r^\alpha\rho\\ r^\alpha\rho u\\ r^\alpha\rho\varepsilon\end{pmatrix}+\frac{\partial}{\partial r}\begin{pmatrix}r^\alpha(\rho u)\\ r^\alpha(\rho u^2+p)\\ r^\alpha\big((\rho\varepsilon+p)u+q\big)\end{pmatrix}=\begin{pmatrix}0\\ \alpha r^{\alpha-1}p\\ r^\alpha\big(W_J+W_{\mathrm{rad}}\big)\end{pmatrix}$$

Conserving when discretized

Los Alamos NATIONAL LABORATORY

# Finite volume 1-D cell definitions

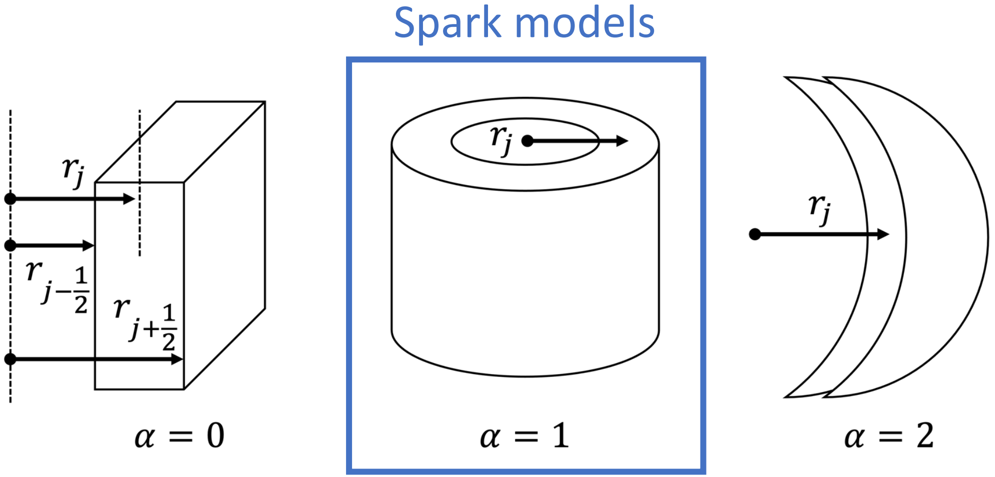


- Finite volume cell average quantities (e.g. mass density $\rho_j$)

$$\rho_j = \frac{1}{\mathcal{V}_j} \int_{r_{j-\frac{1}{2}}}^{r_{j+\frac{1}{2}}} \rho r^\alpha dr, \qquad \mathcal{V}_j = r_{j+\frac{1}{2}}^{\alpha+1} - r_{j-\frac{1}{2}}^{\alpha+1}$$

- Finite volume cell definitions for 1-D
  - $\alpha = 0, 1, 2$ for planar, cylindrical, and spherical
  - Cell index $j = 1, 2, \dots, j_{\max}$
- Cell midpoint

$$r_j = \frac{r_{j+\frac{1}{2}} + r_{j-\frac{1}{2}}}{2}$$

- Cell width

$$\Delta r_j = r_{j+\frac{1}{2}} - r_{j-\frac{1}{2}}$$

Average momentum: $(\rho u)_j$

Average total energy: $(\rho \varepsilon)_j$

# Lagrangian reference frame and flux transformation

- Lagrangian reference frame
  - Cell edges move with material velocity $u$ *evaluated at cell edges*
  - Obtain interfacial quantities using "star region" ($\star$) part of Riemann problem solution

$$\frac{d}{dt} r_{j+\frac{1}{2}} = u^{\star}_{j+\frac{1}{2}}$$

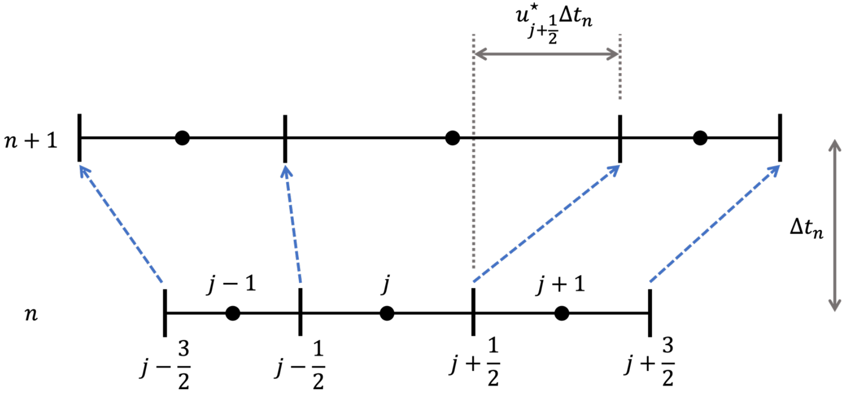


Schematic of Lagrangian mesh moving over one time step

- Flux terms for conserved variables vanish, leaving only acoustic wave terms

$$\frac{1}{r^{\alpha}} \frac{\partial}{\partial r} \left( \begin{matrix} r^{\alpha}(\rho u) \\ r^{\alpha}(\rho u^2 + p) \\ r^{\alpha}((\rho \varepsilon + p) u + q) \end{matrix} \right) \Bigg|_{r=r_{j+\frac{1}{2}}} \rightarrow \frac{1}{r^{\alpha}} \frac{\partial}{\partial r} \left( \begin{matrix} 0 \\ r^{\alpha} p^{\star} \\ r^{\alpha}(p^{\star} u^{\star} + q^{\star}) \end{matrix} \right) \Bigg|_{r=r_{j+\frac{1}{2}}}$$

# Semi-discrete 1-D hydrodynamic equations

- By integrating equations over a cell, $\int_{r_{j-\frac{1}{2}}}^{r_{j+\frac{1}{2}}} \dots dr$, obtain the semi-discretization,

Non-conserving ("NC") form

- *Geometric source term* form,

$$\frac{\partial}{\partial t}\begin{pmatrix}\rho_j \Delta r_j \\ (\rho u)_j \Delta r_j \\ (\rho\varepsilon)_j \Delta r_j\end{pmatrix} + \begin{pmatrix}0 \\ p^\star \\ p^\star u^\star + q^\star\end{pmatrix}\Bigg|_{r=r_{j-\frac{1}{2}}}^{r=r_{j+\frac{1}{2}}} = -\frac{\alpha \Delta r_j}{r_j}\begin{pmatrix}(\rho u)_j \\ (\rho u)_j u_j \\ \left((\rho\varepsilon)_j + p_j\right) u_j + q_j\end{pmatrix} + \Delta r_j \begin{pmatrix}0 \\ 0 \\ W_{J,j} + W_{\mathrm{rad},j}\end{pmatrix}$$

Conserving ("C") form

- *Geometric flux* form,

$$\frac{\partial}{\partial t}\begin{pmatrix}\rho_j \mathcal{V}_j \\ (\rho u)_j \mathcal{V}_j \\ (\rho\varepsilon)_j \mathcal{V}_j\end{pmatrix} + \begin{pmatrix}0 \\ r^\alpha p^\star \\ r^\alpha (p^\star u^\star + q^\star)\end{pmatrix}\Bigg|_{r=r_{j-\frac{1}{2}}}^{r=r_{j+\frac{1}{2}}} = \begin{pmatrix}0 \\ \Pi_j \\ \mathcal{V}_j\left(W_{J,j} + W_{\mathrm{rad},j}\right)\end{pmatrix}$$

Evaluate analytically given $p = p(r)$ over cell $\Rightarrow$ $\Pi_j = \alpha \int_{r_{j-\frac{1}{2}}}^{r_{j+\frac{1}{2}}} p r^{\alpha-1} dr$

# Lagrangian mesh update and time discretization

- Consider time step from $t_n \to t_{n+1}$ with $\Delta t_n = t_{n+1} - t_n$ and $n = 0, 1, \dots, n_{\max}$
- For hydrodynamic equations, discretize in time with forward (**explicit**) Euler
- Lagrangian mesh update step

$$r_{j+\frac{1}{2},n+1} = r_{j+\frac{1}{2},n} + u^{\star}_{j+\frac{1}{2},n} \Delta t_n$$

- Ex: time derivative terms in conservation equations,

$$\frac{\partial}{\partial t}\begin{pmatrix} \rho_j \mathcal{V}_j \\ (\rho u)_j \mathcal{V}_j \\ (\rho \varepsilon)_j \mathcal{V}_j \end{pmatrix} \to \frac{1}{\Delta t_n}\begin{pmatrix} \rho_{j,n+1}\mathcal{V}_{j,n+1} - \rho_{j,n}\mathcal{V}_{j,n} \\ (\rho u)_{j,n+1}\mathcal{V}_{j,n+1} - (\rho u)_{j,n}\mathcal{V}_{j,n} \\ (\rho \varepsilon)_{j,n+1}\mathcal{V}_{j,n+1} - (\rho \varepsilon)_{j,n}\mathcal{V}_{j,n} \end{pmatrix}$$

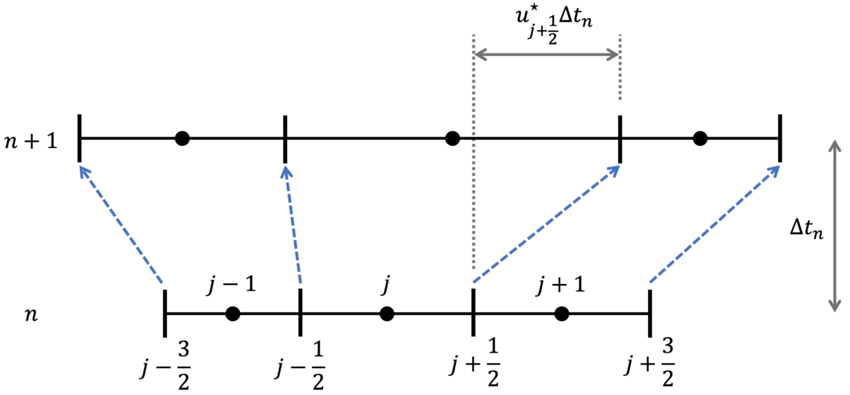


Schematic of Lagrangian mesh moving over one time step

Stable for CFL criterion,

$$\Delta t_n < \min_j \left( \frac{\Delta r_{j,n}}{|u_{j,n} + c_{j,n}|} \right)$$

$c$: sound speed

# Riemann solver and piecewise-linear spatial reconstruction of variables

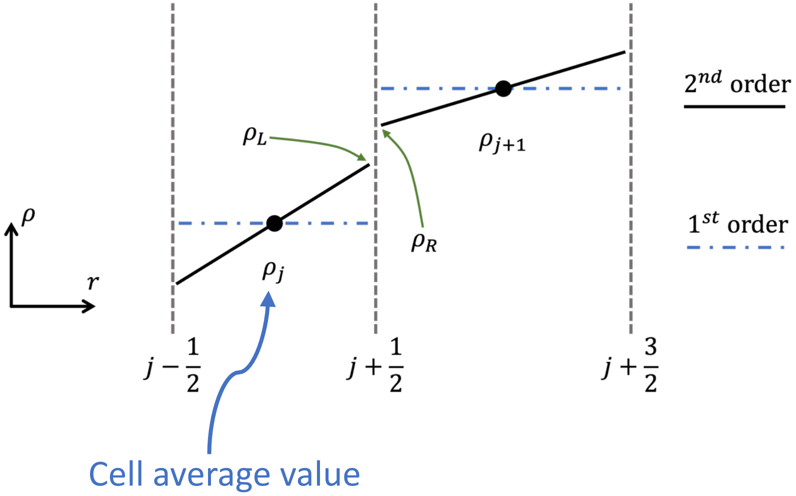


Heat conduction flux,

$$q^{\star}_{j+\frac{1}{2}} = -\kappa^{\star}_{j+\frac{1}{2}} \frac{T_{j+1}-T_j}{r_{j+1}-r_j}$$

- Find cell edge velocity and pressure with Primitive Variable Riemann Solver (Toro, 1999)
  - $u^{\star} = \dfrac{\rho_R u_R c_R + \rho_L u_L c_L + (p_L - p_R)}{\rho_R c_R + \rho_L c_L}$
  - $p^{\star} = \dfrac{\rho_R c_R p_L + \rho_L c_L p_R + \rho_R \rho_L c_R c_L (u_L - u_R)}{\rho_R c_R + \rho_L c_L}$
- Piecewise-linear reconstruction for primitive variables $\rho$, $u$, $p$, $c$
  - $\rho_L = \rho_j + \frac{\Delta r_j}{2} \delta\rho_j$
  - $\rho_R = \rho_{j+1} - \frac{\Delta r_{j+1}}{2} \delta\rho_{j+1}$
- Slopes $\delta\rho_j$ monotonically-limited using van Albada limiter function

# Eddington (P1) moment approximation to the radiative transfer equation

- General form of radiative transfer equation:
- $\frac{1}{c_0}\frac{\partial \mathcal{I}_\nu}{\partial t} + \Omega \cdot \nabla \mathcal{I}_\nu = \frac{1}{\lambda_\nu}\left(\mathcal{I}_{\nu,p} - \mathcal{I}_\nu\right)$
  - $\mathcal{I}_\nu$ is the spectral intensity, a function $\mathcal{I}_\nu = \mathcal{I}_\nu(\Omega, r, t)$ of **direction $\boldsymbol{\Omega}$, position $\boldsymbol{r}$, and time $\boldsymbol{t}$**, while $\mathcal{I}_{\nu,p} = \frac{2h\nu^3}{c_0^2}\frac{1}{e^{h\nu/kT}-1}$ is the **Planckian** (equilibrium) spectral intensity
- Expand in spherical harmonics, integrate over all directions and frequencies (moment expansion), apply “gray-body” assumption for freq. dependence
- Obtain for first moment the Eddington/P1 approximation (similar to two-term Boltzmann approximation):
- $\boxed{\frac{\partial}{\partial t}(\rho\varepsilon_{\mathrm{rad}}) + \frac{1}{r^\alpha}\frac{\partial}{\partial r}(r^\alpha q_{\mathrm{rad}}) = -W_{\mathrm{rad}}}$

$$\boxed{\begin{aligned} q_{\mathrm{rad}} &= -\lambda_{\mathrm{rad}}\frac{c_0}{3}\frac{\partial}{\partial r}(\rho\varepsilon_{\mathrm{rad}}) \\ W_{\mathrm{rad}} &= \frac{c_0}{\lambda_{\mathrm{rad}}}(\rho\varepsilon_{\mathrm{rad}} - \rho\varepsilon_{\mathrm{bb}}) \end{aligned}}$$

Blackbody energy density

$$\rho\varepsilon_{\mathrm{bb}} = \frac{4\varsigma T^4}{c_0}$$

Los Alamos NATIONAL LABORATORY

# Eddington (P1) moment approximation to the radiative transfer equation, time-implicit discretization

- Obtain semi-discrete form similar to conservative "C" form of hydrodynamic equations,

$$\frac{1}{c_0}\frac{\partial}{\partial t}\left((\rho\varepsilon_{\mathrm{rad}})_j\mathcal{V}_j\right)+\left(r^\alpha\frac{q^\star_{\mathrm{rad}}}{c_0}\right)\Bigg|_{r=r_{j-\frac{1}{2}}}^{r=r_{j+\frac{1}{2}}}=\frac{\mathcal{V}_j}{\lambda_{\mathrm{rad},j}}\left((\rho\varepsilon_{\mathrm{bb}})_j-(\rho\varepsilon_{\mathrm{rad}})_j\right)$$

Tridiagonal linear system

- Discretize in time with backward (implicit) Euler to avoid stability restrictions on time step (i.e. speed of light $c_0$ is large compared to other speeds of interest)
- Radiation energy flux at cell edges,

$$q^\star_{\mathrm{rad},j+\frac{1}{2}}=-\lambda^\star_{\mathrm{rad},j+\frac{1}{2}}\frac{c_0}{3}\frac{(\rho\varepsilon_{\mathrm{rad}})_{j+1}-(\rho\varepsilon_{\mathrm{rad}})_j}{r_{j+1}-r_j}$$

- $\lambda^\star_{\mathrm{rad},j+\frac{1}{2}}$ found using harmonic mean of cell center values

# Circuit equations and discretization

- Joule heating term: $W_J = \sigma E^2$ where $E = \frac{IR_s}{\ell}$
- Spark resistance: $R_s = \frac{\ell}{2\pi \int_0^\infty \sigma \, r \, dr}$
- Circuit equations: $\frac{dQ}{dt} = -I, \qquad \frac{dI}{dt} = -\frac{(R_s+R_v)I}{L} + \frac{Q}{LC}$
- Numerical integration for spark resistance (couples hydrodynamic and circuit models):

$$R_{s,n} = \frac{\ell}{2\pi \sum_{j=1}^{j_{\max}} \sigma_{j,n} r_{j,n} \Delta r_{j,n}}$$

- Circuit ODE system discretized using classical Crank-Nicolson (implicit) scheme

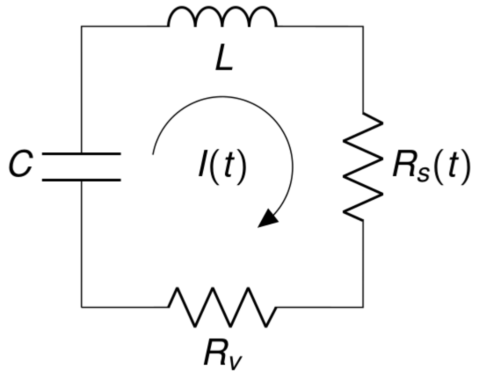


Series RLC model of ESD between conductors

Los Alamos NATIONAL LABORATORY

# Verification of hydrodynamics with Sedov blast wave self-similar solution

- Instantaneous deposition of energy in infinitesimal volume
  - Strong shock wave propagates in medium of uniform density, zero ambient pressure
  - Ideal gas $p = (\gamma - 1)\rho e$
  - $\gamma = \frac{7}{5} = 1.4$ for *ideal* diatomics
  - Cylindrical case relevant to sparks
- Self-similar profiles for density, velocity, and pressure
- Verifies implementation of inviscid, non-conducting hydrodynamics

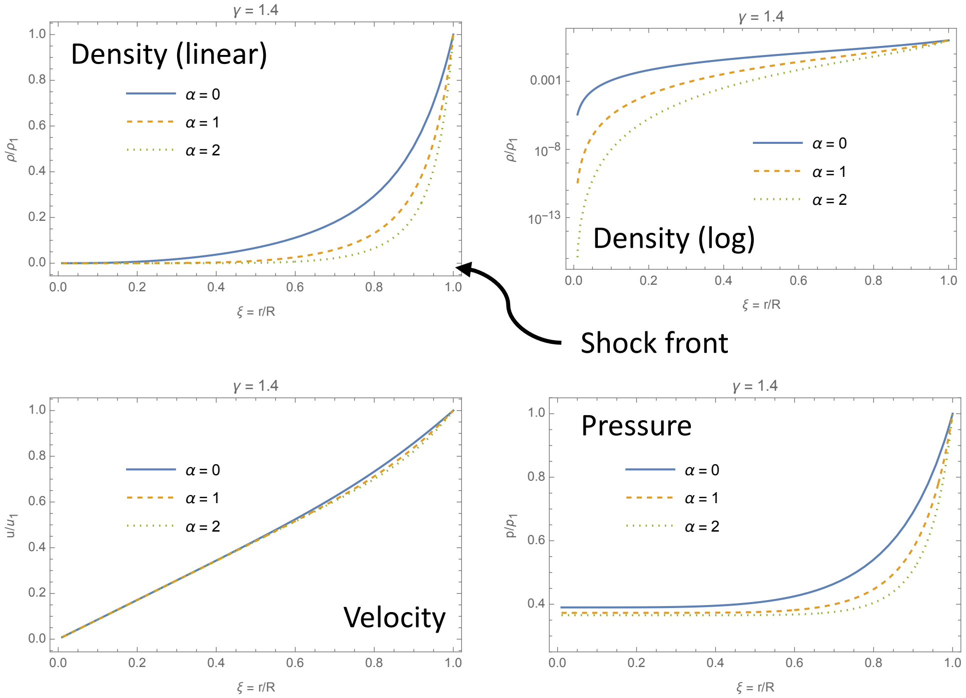


Planar, cylindrical, and spherical: $\alpha = 0, 1, 2$

# Sedov blast wave verification results (cylindrical)

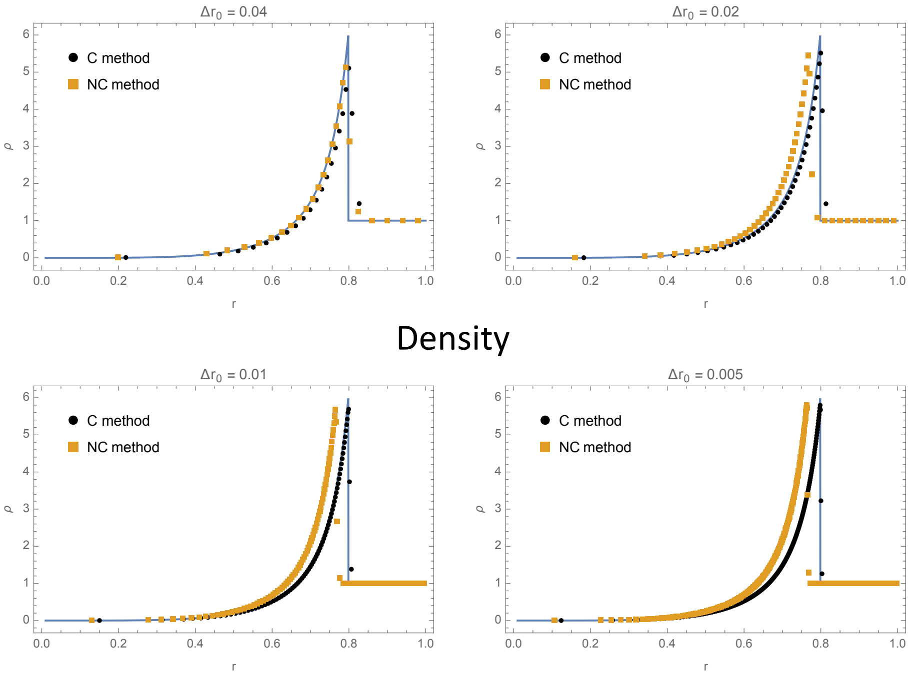


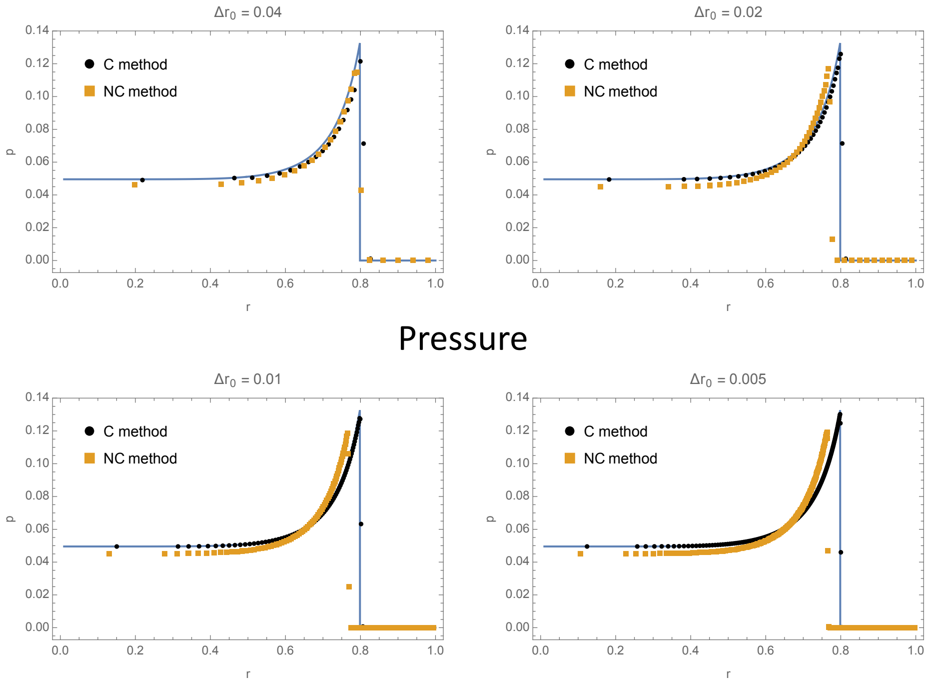


- “C” scheme converges about 1st order as initial mesh size decreased
- “NC” converges to wrong shock position

Los Alamos NATIONAL LABORATORY

# Sedov blast wave verification results (cylindrical)

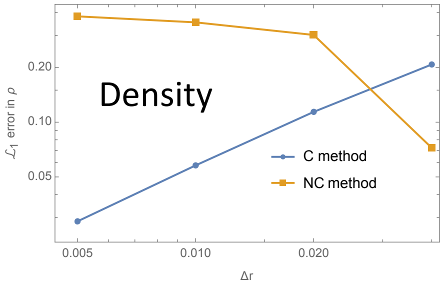


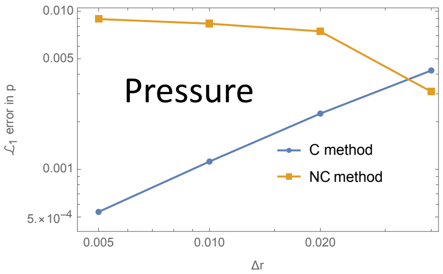


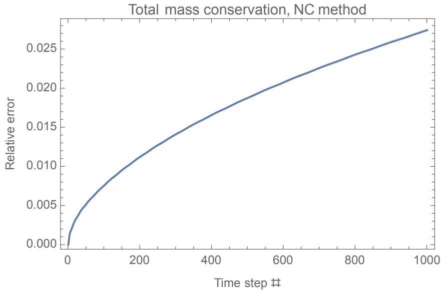


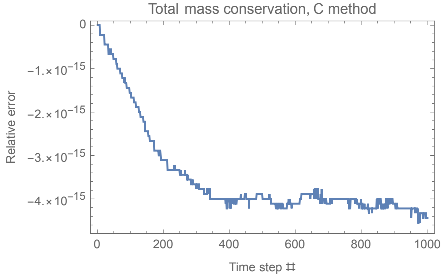


- $\mathcal{L}_1$ norm used for estimate of 1st order convergence
- Total mass and energy conservation errors shows “C” scheme conserves within machine precision, “NC” scheme has several percent error

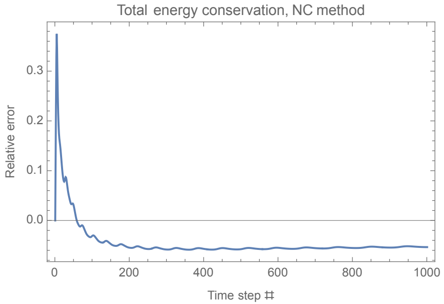


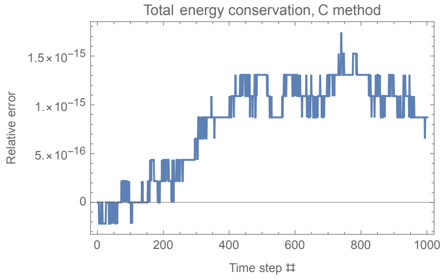


Los Alamos NATIONAL LABORATORY

# Heat conduction verification, nonlinear diffusion similarity solution

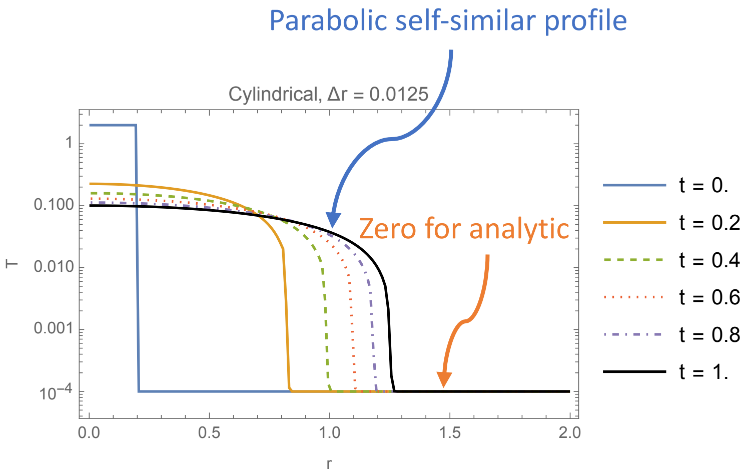


Numerical "C" scheme for cylindrical case at highest mesh resolution

- Temperature-dependent thermal conductivity, $\kappa = 2\chi_0 T$
- Constant thermal diffusivity, $\beta = \frac{\chi_0}{\rho c_p}$
- In absence of flow ($u = 0$, $p = 0$), energy conservation equation becomes nonlinear diffusion equation,

$$\frac{\partial T}{\partial t} = 2\beta \frac{1}{r^\alpha}\frac{\partial}{\partial r}\left(r^\alpha T \frac{\partial T}{\partial r}\right)$$

- Solution (Barenblatt and others) is a parabolic self-similar profile in dimensionless coordinate $\xi = r/r_f$

# Heat conduction verification, cylindrical results

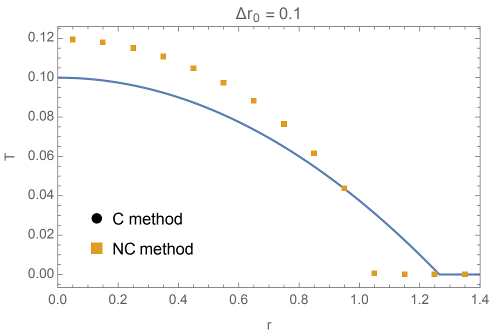


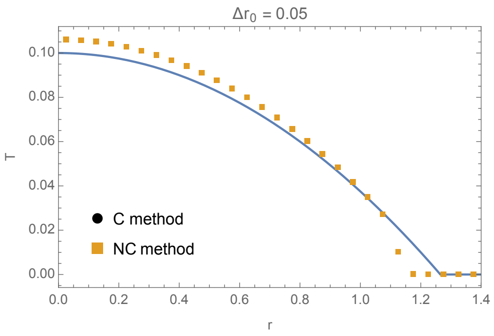


Temperature at time $t = 1$

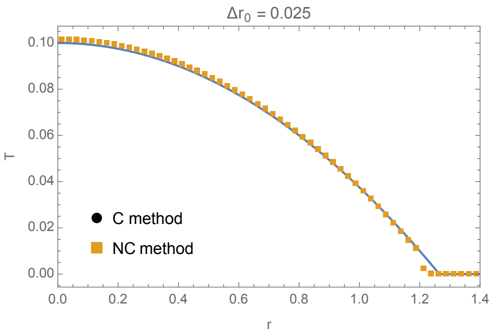


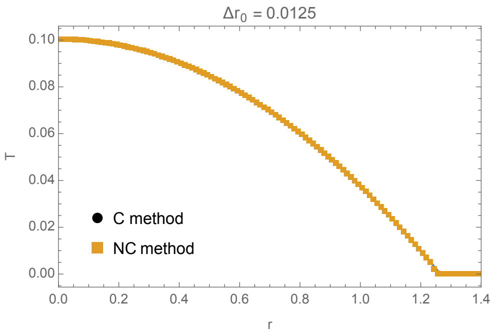


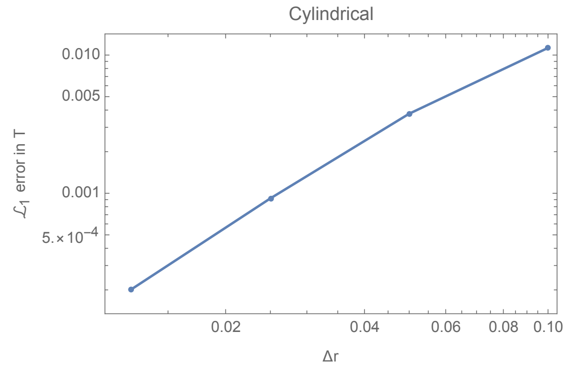


- "C" and "NC" schemes identical to machine precision *for the cylindrical case*
- 2[nd] order convergence in $\mathcal{L}_1$ norm for temperature
- Verifies heat conduction independently of hydrodynamics

# Verification of Eddington/P1 approximation for radiative transfer (steady-state)

- Because speed of light $c_0 \gg c$ (sound speed), parabolic P1 approximation behaves like elliptic equation for spark timescales
  - Hence implicit time-discretization
- Steady-state gives ODE, $\frac{d}{dx}\left(x^\alpha \frac{du}{dx}\right) = \mathrm{a}x^\alpha(u - b)$
- With mappings $r \to x$, $\rho\varepsilon_{\mathrm{rad}} \to u$, $\frac{3}{\lambda_{\mathrm{rad}}^2} \to \mathrm{a}$, and $\rho\varepsilon_{\mathrm{bb}} \to b$
- Analytical solutions for source

$$b(x) = \begin{cases} b_0, & x \leq 1 \\ 0, & x > 0 \end{cases}$$

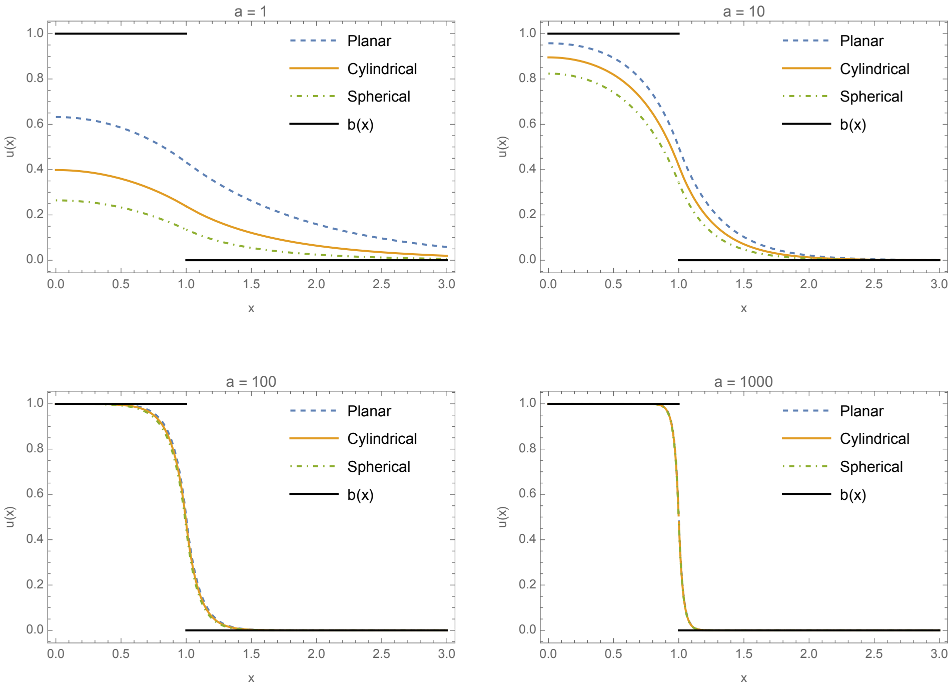


Analytical solutions for $b_0 = 1$, various values of $\mathrm{a} = \frac{3}{\lambda_{\mathrm{rad}}^2}$

Los Alamos NATIONAL LABORATORY

# Verification of Eddington/P1 approximation for radiative transfer, results

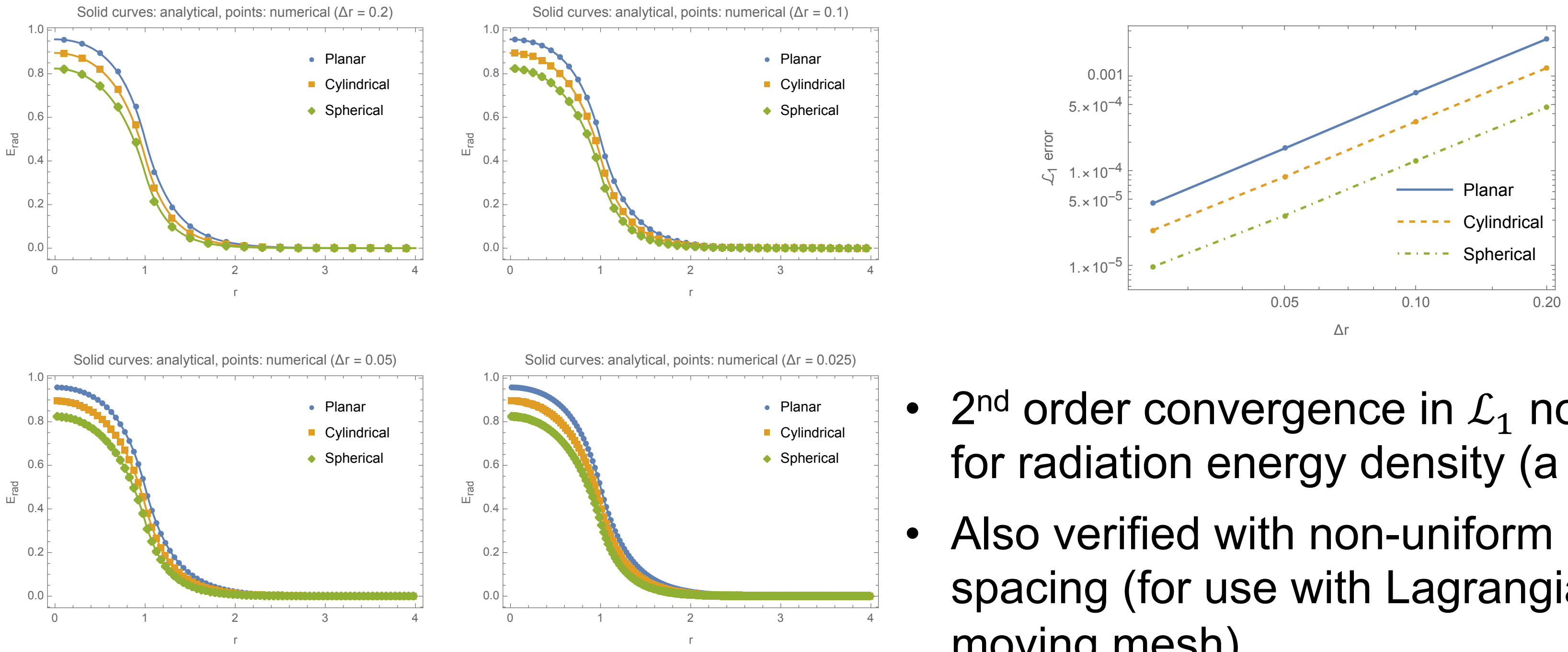


- $2^{nd}$ order convergence in $\mathcal{L}_1$ norm for radiation energy density (a = 10)
- Also verified with non-uniform grid spacing (for use with Lagrangian moving mesh)

# Air Equation of State (EOS)

# Analytic fit for air EOS

- Fit to existing tabular data generated by Magpie thermodynamic composition code
- EOS form of $p = \Gamma \rho e$, where $\Gamma = \Gamma(\rho, e)$ is a simple analytic function of $\rho$ and $e$
  - Think ideal gas law where $\gamma - 1 = \Gamma$ is *not constant*
  - Less computational effort than interpolating tabular data directly
  - Well-behaved asymptotes
  - Analytic sound speed $c$

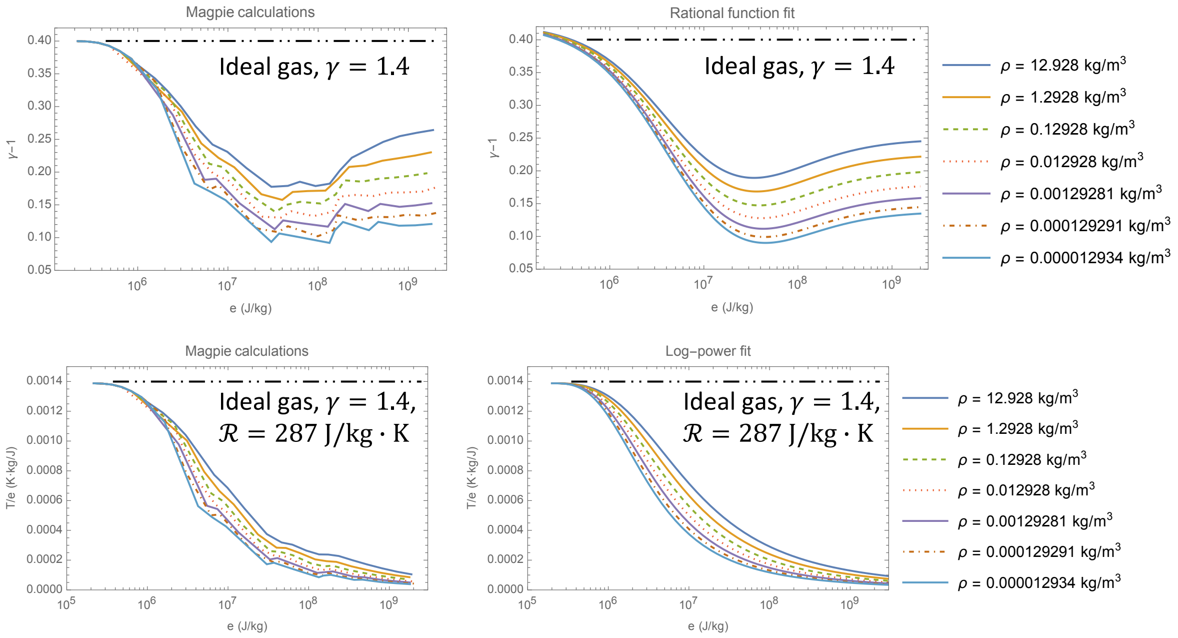


$$c = \sqrt{\frac{\partial p}{\partial \rho} + \frac{p}{\rho^2}\frac{\partial p}{\partial e}}$$

# Analytic fit for air EOS, temperature

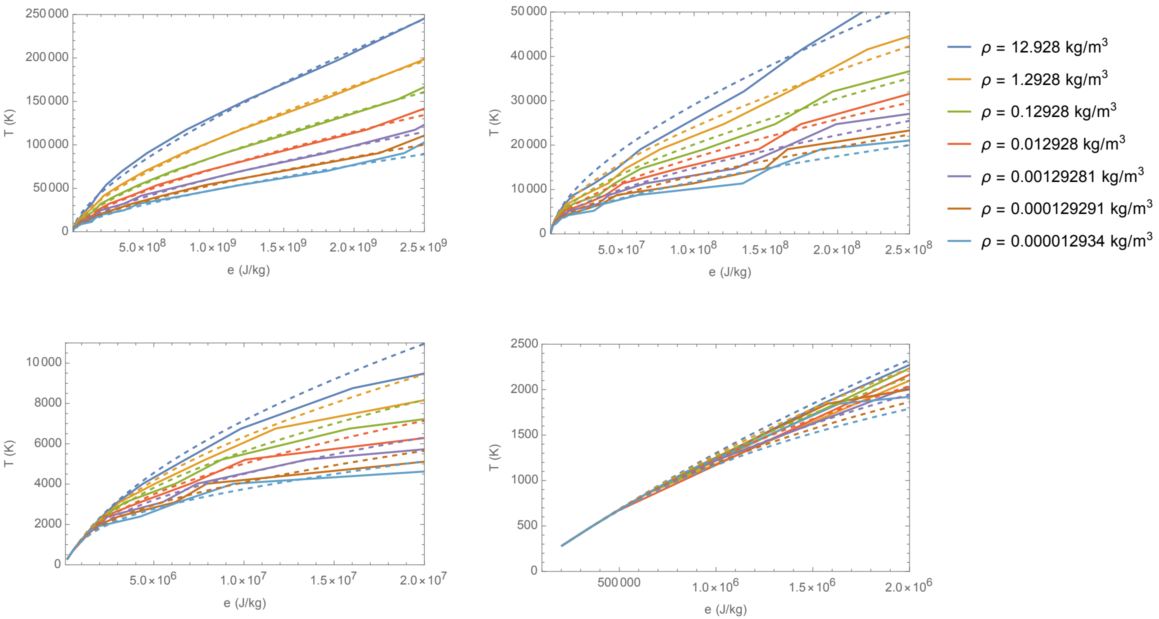


- Temperature fit of the form $T = e/\mathcal{C}$ with $\mathcal{C} = \mathcal{C}(\rho, e)$, not to be confused with sound speed $c$
- Fit form and coefficients chosen for best fit to temperatures above $T \approx 20{,}000\ \mathrm{K}$
  - Important for radiative transfer accuracy ($T^4$ dependence)

# Analytic fit for air EOS, relative error

- Relative error for temperature and pressure generally within 10-15 %, with exception of extreme isochore (density) values.
- Very low error for lower energies (correct asymptote to ideal gas)
  - Temperature has very low error for high int. energy

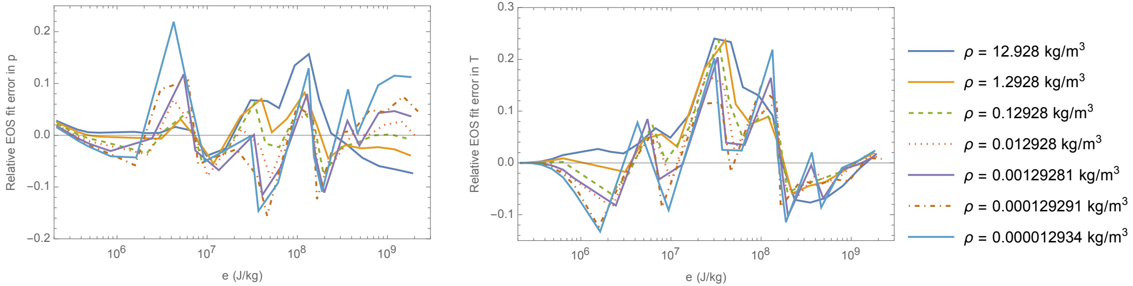


$p = p(\rho, e)$

$$p = \Gamma \rho e$$

$$\Gamma = \Gamma_0 + \frac{e/e_1}{(e/e_1)+1}\left(\Gamma_1 + \delta\Gamma \frac{(\rho/\rho_0)^g - 1}{(\rho/\rho_0)^g + 1}\right) + \frac{e/e_2}{(e/e_2)+1}\Gamma_2$$

| $\Gamma_0$ | $\Gamma_1$ | $\Gamma_2$ | $\delta\Gamma$ | $e_1$ (J/kg) | $e_2$ (J/kg) | $g$ | $\rho_0$ (kg/m$^3$) |
|---|---|---|---|---|---|---|---|
| 0.425279 | −0.350109 | 0.147782 | 0.104274 | $4.4756 \times 10^6$ | $6.58144 \times 10^7$ | 1/5 | 1 |

$$T = \frac{e}{\mathcal{C}}$$

$$\mathcal{C} = \mathcal{C}_0 + \frac{1}{(\rho/\rho_0)^h + 1}\left(\mathcal{C}_1 + \delta\mathcal{C}\frac{1}{(\rho/\rho_0)^h + 1}\right)\mathscr{L}^3\left(\frac{e}{e_0}\right)$$

$$\mathscr{L}(x) = \begin{cases} \log(x) & x \geq 1 \\ 0 & x < 1 \end{cases},$$

| $\mathcal{C}_0$ (J/(kg·K)) | $\mathcal{C}_1$ (J/(kg·K)) | $\delta\mathcal{C}$ (J/(kg·K)) | $e_0$ (J/kg) | $h$ | $\rho_0$ (kg/m$^3$) |
|---|---|---|---|---|---|
| 720.6 | 2.45959 | 53.7537 | $2 \times 10^5$ | 1/10 | 1 |

$T = T(\rho, e)$

# Air EOS isentropic sound speeds and shock Hugoniot

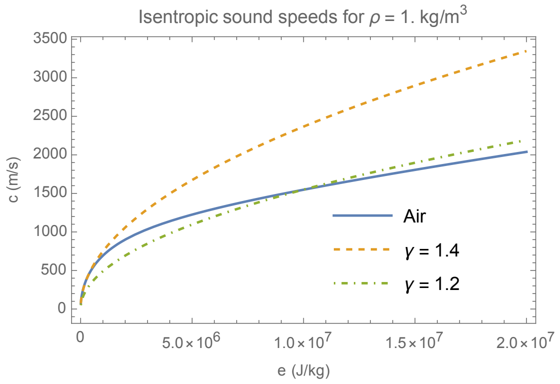


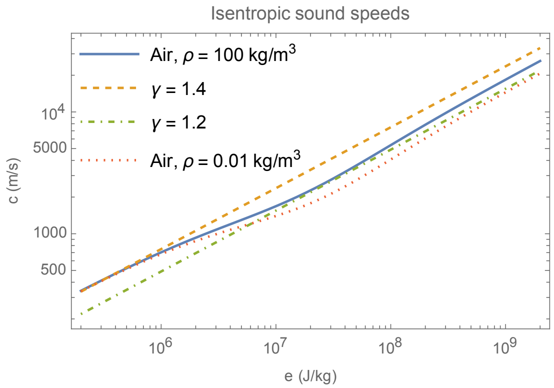


$$c = \sqrt{\frac{\partial p}{\partial \rho} + \frac{p}{\rho^2}\frac{\partial p}{\partial e}}$$

Density ratio

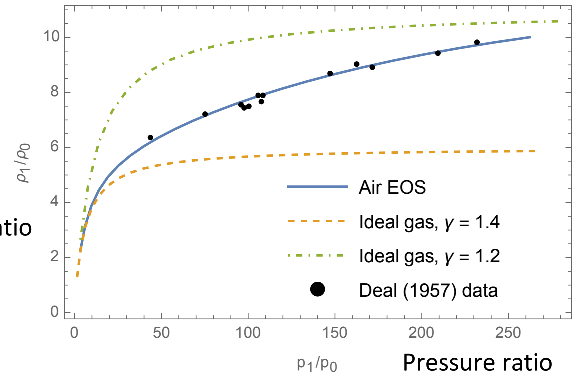


Pressure ratio

- Sound speed correctly asymptotes to ideal gas value ($\gamma = 1.4$) at low energies/temperatures
  - Mild density-dependence at higher energies
- Air EOS fit validated for intermediate-strength shock data of Deal (1957, at LANL)
  - Shock propagates with correct speed and jump values for variables

Los Alamos NATIONAL LABORATORY

# Seed conductivity, transport properties, and parameter sensitivity studies

# Transport properties for spark discharge model

- Mean free path (MFP) for radiative transport, gray-body approximation
  - At temperatures $k_B T \approx 5\ \mathrm{eV}$, peak of Planck spectral intensity in photoionizing region
  - Constant cross section approximation, $\boxed{\lambda_{\mathrm{rad}} = \frac{\lambda_0 \rho_0}{\rho}}$
  - Atmospheric air ($\rho_0 = 1.2\ \frac{\mathrm{kg}}{\mathrm{m}^3}$) values, $\lambda_0 \approx 10 - 20\ \mu\mathrm{m}$
- Thermal conductivity found via Wiedemann-Franz relation (for Maxwell-Boltzmann distribution for electrons), $\boxed{\kappa = 2\left(\frac{k_B}{e}\right)^2 \sigma_{\mathrm{eq}} T}$
- Equilibrium electrical conductivity $\sigma_{\mathrm{eq}}$ found from approximate mixing rule for electron-neutral and electron-ion collision frequencies
- $\boxed{\sigma_{\mathrm{eq}} = \frac{e^2 n_e}{m_e \nu_e} \approx \frac{e^2}{m_e \bar{u}_e} \frac{\Upsilon_{\mathrm{ion}}}{(1-\Upsilon_{\mathrm{ion}})\Xi_0 + \Upsilon_{\mathrm{ion}} \Xi_{\mathrm{ion}}}}$ $\quad \bar{u}_e = \sqrt{\frac{8 k_B T}{\pi m_e}},\ \Xi_{\mathrm{ion}} = \left(\frac{\pi x_0 \mathcal{E}_{\mathrm{ion},H}}{2 k_B T}\right)^2 \ln \Lambda$

*Ionization fraction $\Upsilon_{\mathrm{ion}} \in [0,1]$ found from simplified Saha equation

Los Alamos NATIONAL LABORATORY

# Seed conductivity for finite initial conductivity

- Problem: $\sigma_{\mathrm{eq}}$ negligible at room temperature
- Solution: conductivity accounting for non-equilibrium "seed" electrons produced by initial breakdown process: $\boxed{\sigma = \sigma_{\mathrm{eq}} + \sigma_s}$
- Treat $\sigma_s$ as conserved scalar:

$$\boxed{\frac{\partial}{\partial t}\sigma_s + \frac{1}{r^\alpha}\frac{\partial}{\partial r}(r^\alpha \sigma_s u) = 0}$$

- Solve with rest of hydrodynamic equations
  - $\sigma_s = e n_{e,s} \mu_e$ where $\mu_e$ is a constant
  - $\sigma \approx \sigma_{eq}$ after spark reaches temperatures associated with peak current
- "C" scheme discretization: $\sigma_{s,j,n+1} = \sigma_{s,j,n} \dfrac{\mathcal{V}_{j,n}}{\mathcal{V}_{j,n+1}}$

Novel aspect: most models use localized pre-heating to give finite initial conductivity

Initial conditions for sensitivity study:

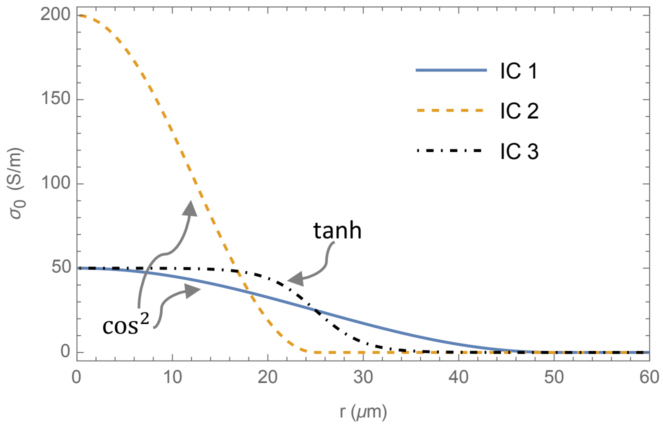


$$R_{s,0} \approx 30\ \mathrm{k\Omega}$$

# Seed conductivity initial condition study, results for circuit variables

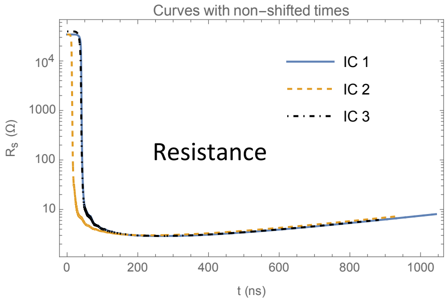


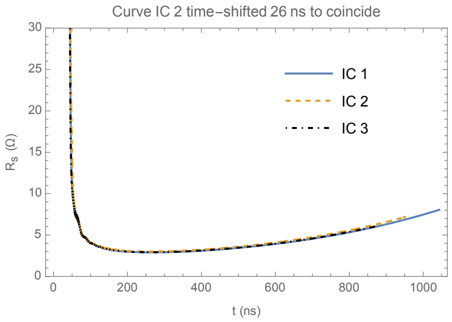


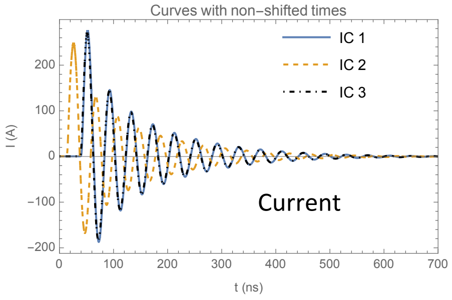


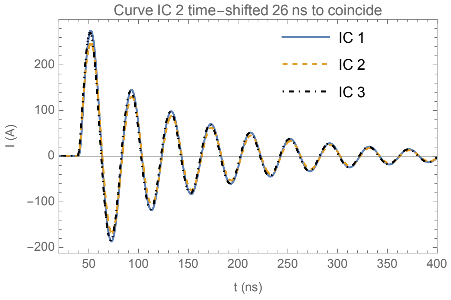


- Minor differences in current and spark resistance between IC's
  - IC2 time-shifted earlier since higher value of $\sigma_s$ on axis initially lead to initially faster heating
- (In)sensitive to small perturbations in seed conductivity initial condition
- Validates use of seed conductivity to initiate Joule heating
- Reference values for this and other sensitivity studies presented:

| $\log\Lambda$ | $\lambda_0\,(\mu\mathrm{m})$ | $\rho_0\,(\mathrm{kg/m^3})$ | $\ell\,(\mathrm{mm})$ | $\varphi_0\,(\mathrm{kV})$ | $R_v\,(\Omega)$ | $L\,(\mathrm{nH})$ | $C\,(\mathrm{pF})$ |
|---|---|---|---|---|---|---|---|
| 10 | 10 | 1.2 | 4 | 12 | 0.1 | 200 | 200 |

# Seed conductivity initial condition study, results for hydrodynamic variables

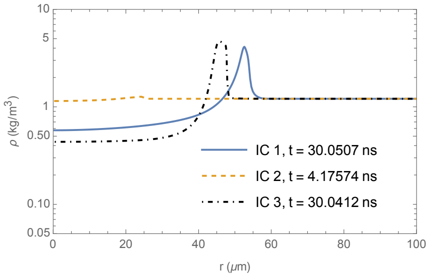


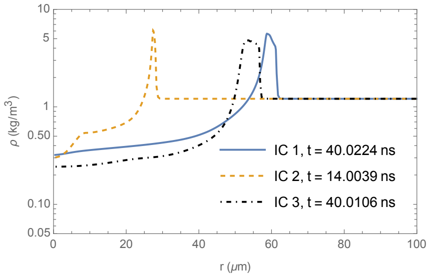


Density

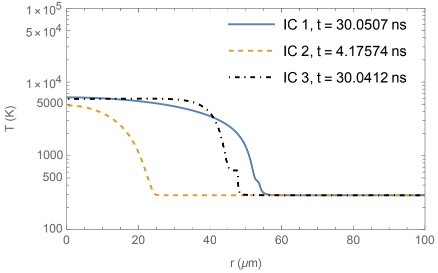


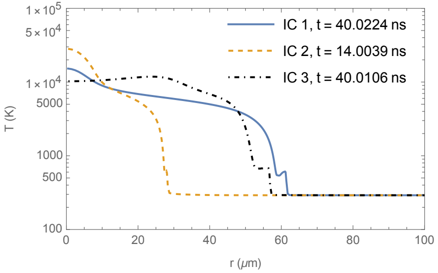


Temperature

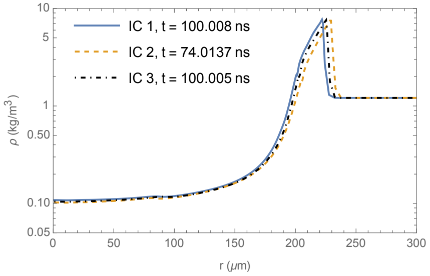


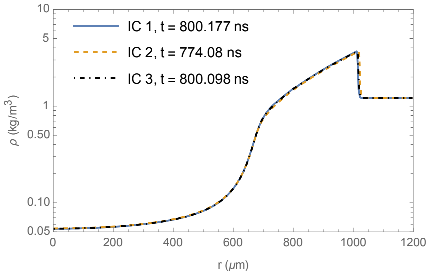


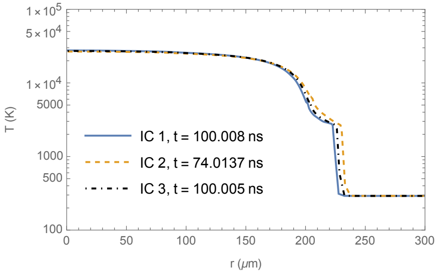


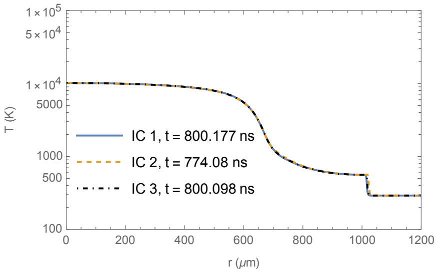


- Effects of initial conditions disappear at later times, as expected for same energy deposition

Los Alamos NATIONAL LABORATORY

# Conductivity study, effect of varying Coulomb log parameter on circuit variables

- $\ln\Lambda$ treated as constant in electron-ion cross section $\Xi_{\text{ion}} = \left(\frac{\pi x_0 \mathcal{E}_{\text{ion},H}}{2k_B T}\right)^2 \ln\Lambda$
- Range of approximately $5 \le \ln\Lambda \le 15$ for most plasma conditions
- Idea: treat $\ln\Lambda$ as parameter to study sensitivity of model to conductivity
- Result: minimum value of spark resistance $R_{s,\min}$ strongly affected, but *rate of recovery* from $R_{s,\min}$ only weakly affected

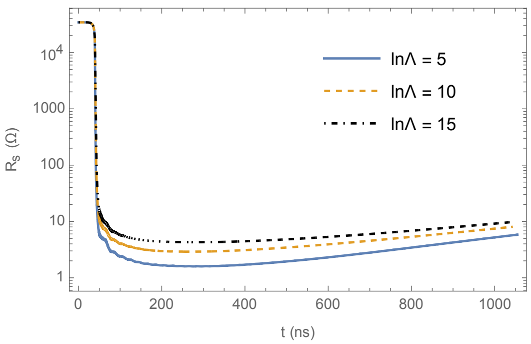


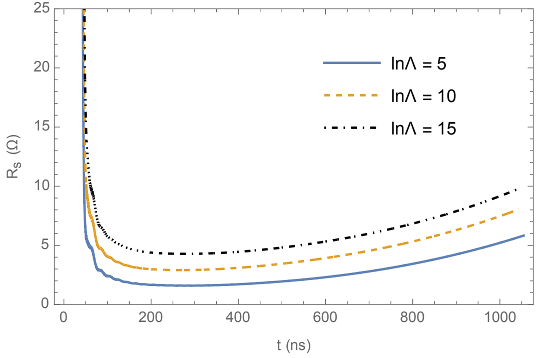


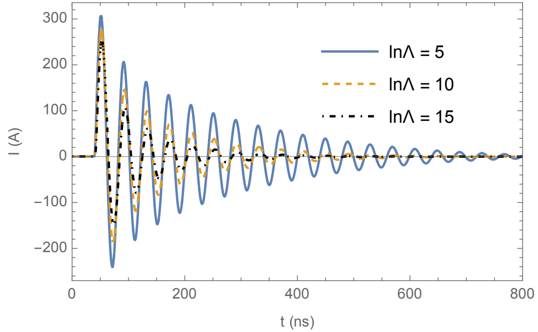

# Conductivity study, effect of varying Coulomb log parameter on density and pressure

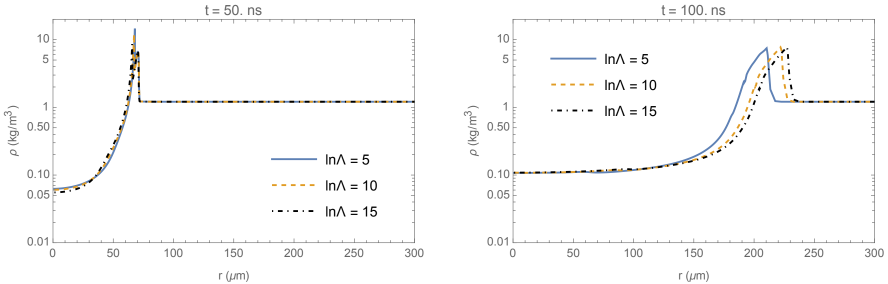


Density

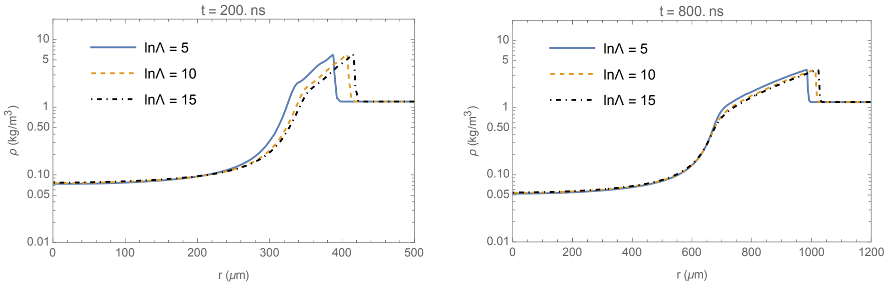


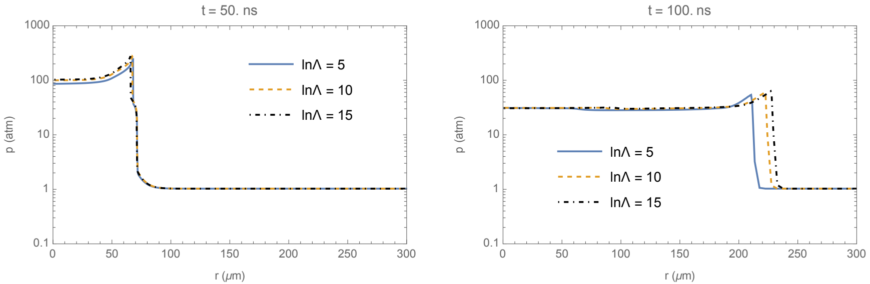


Pressure

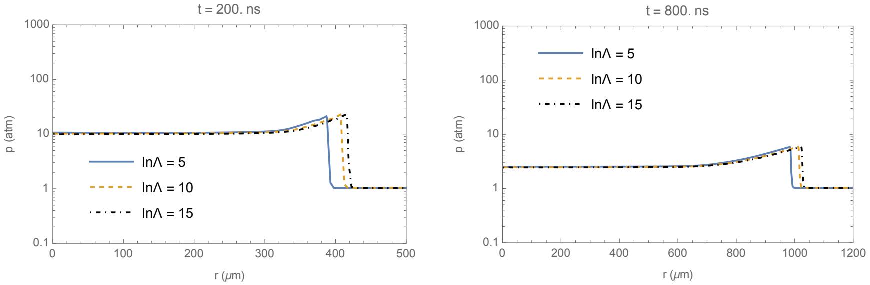


- Higher $R_{s,\min}$ due to higher $\ln\Lambda$ leads to more energy deposition in spark
- Faster shock propagation

Los Alamos NATIONAL LABORATORY

# Conductivity study, effect of varying Coulomb log parameter on temperature

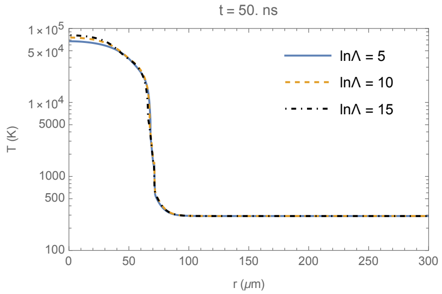


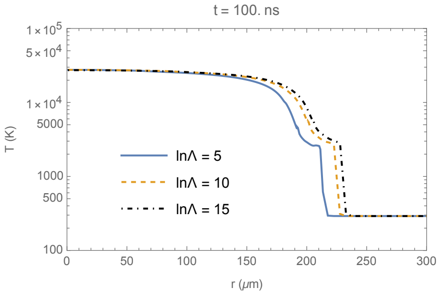


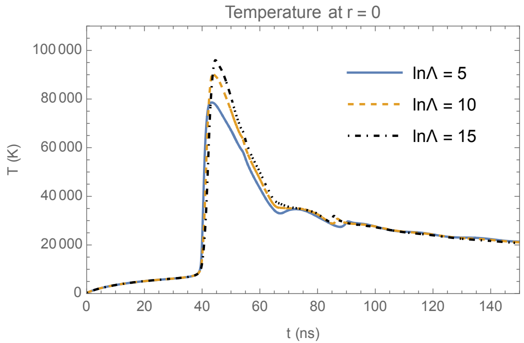


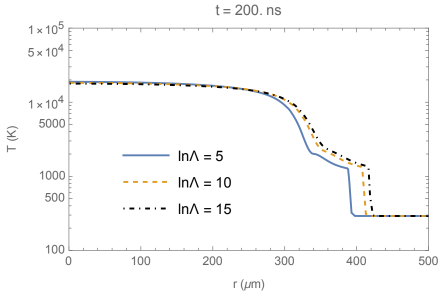


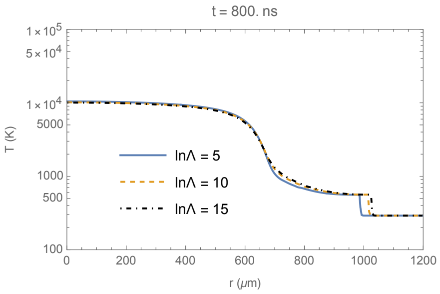


- Higher $R_{s,\min}$ due to higher $\ln\Lambda$ leads to more energy deposition in spark
- Higher peak temperatures near axis of symmetry

# Radiative MFP study, effects on circuit variables

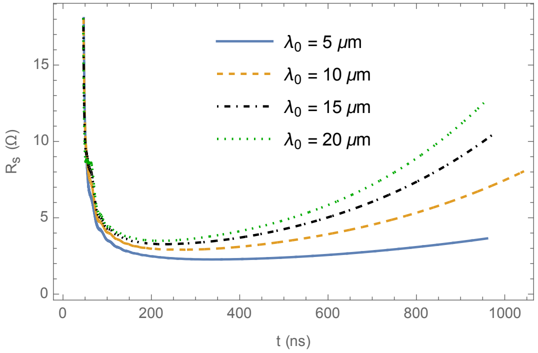


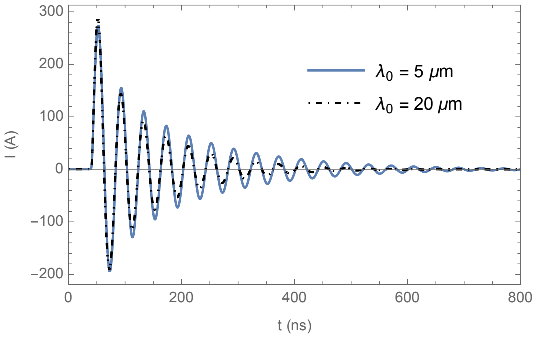


- Vary radiative MFP for ambient atmospheric conditions, $\lambda_0$
- Vary over range $5\mu\mathrm{m} \leq \lambda_0 \leq 20\mu\mathrm{m}$
- Weakly affects minimum spark resistance
- Longer $\lambda_0$ increases rate at which $R_s$ recovers from $R_{s,\min}$
  - Faster cooling during later stages of discharge
  - More complex behavior than other parameters varied in these studies

# Radiative MFP study, effects on density

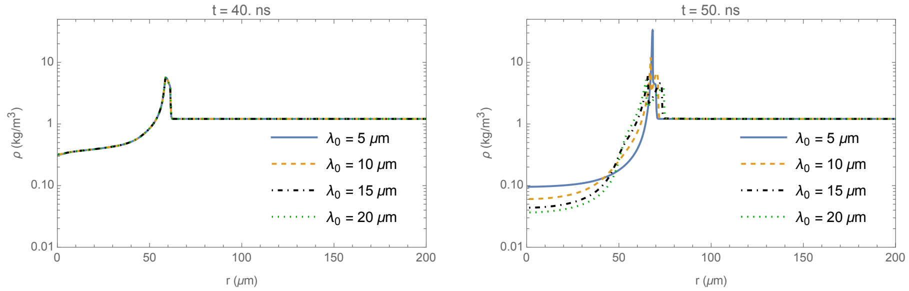


- Density on axis lower for larger $\lambda_0$ at earlier times, but reversed trend at later times
- Analogous trends observed for temperature

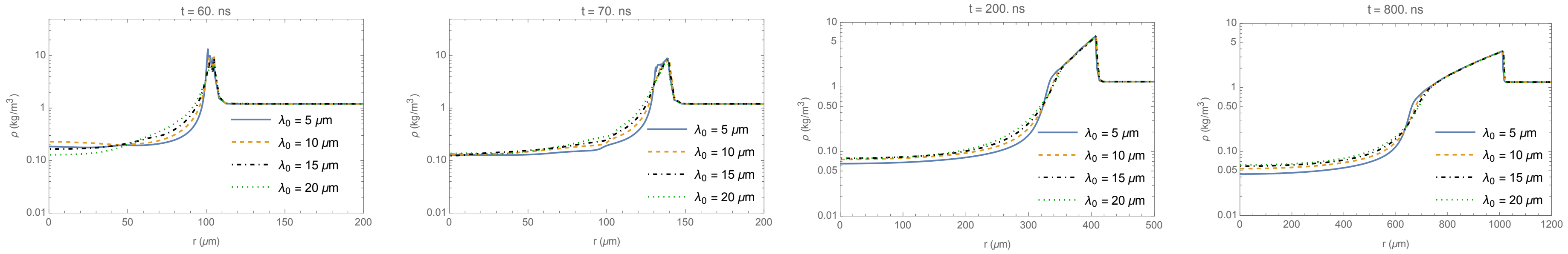


Los Alamos
NATIONAL LABORATORY

# Radiative MFP study, effects on pressure

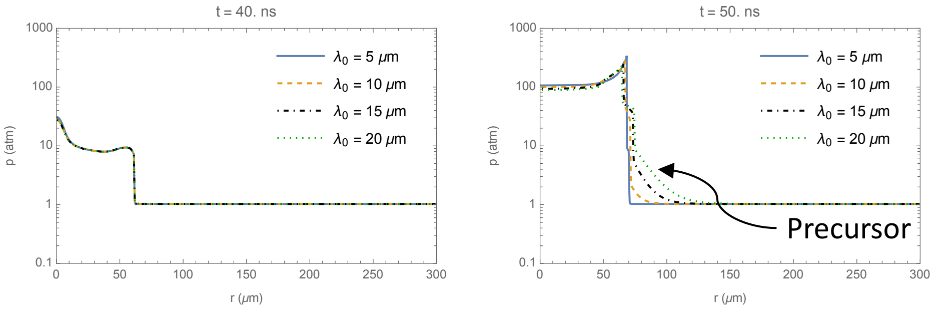


- Longer $\lambda_0$ leads to radiative precursor (heating ahead of shock)
  - Occurs only around peak current
- Pressure otherwise independent of varying $\lambda_0$

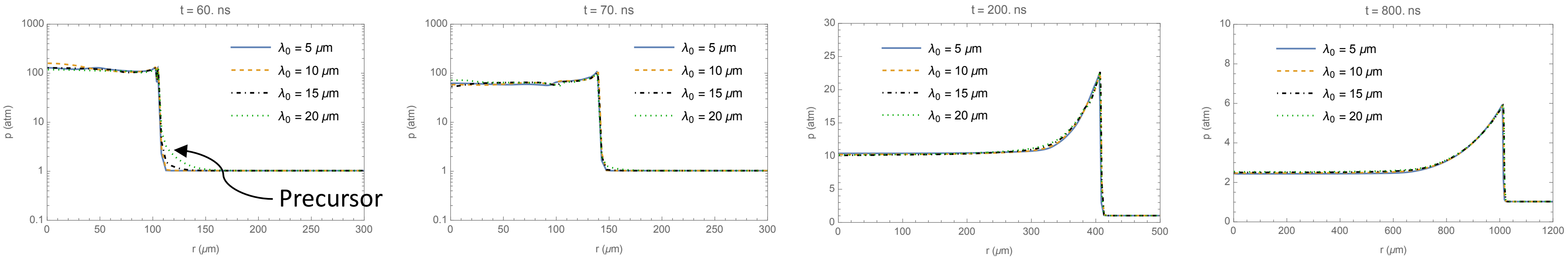

# Radiative MFP study, effects on temperature

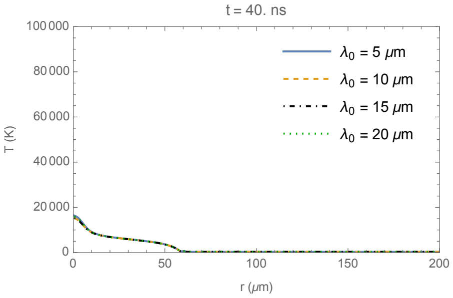


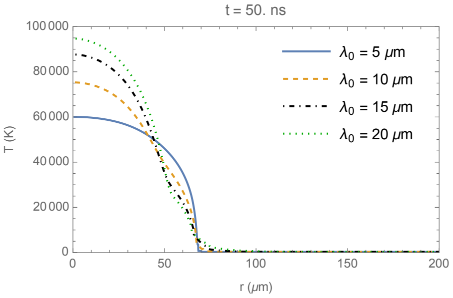


- Temperature on axis *higher* for larger $\lambda_0$ at earlier times, but *reversed* trend at later times
  - More effective cooling during later stages of discharge
  - Opposite behavior to density (consistent with pressure mostly independent of $\lambda_0$)

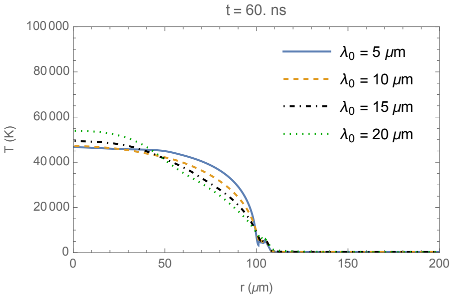


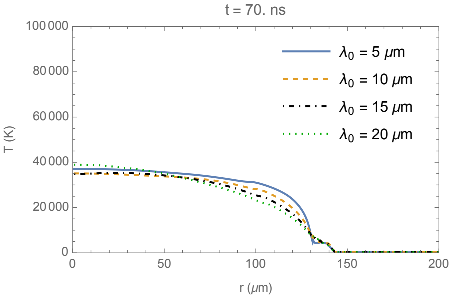


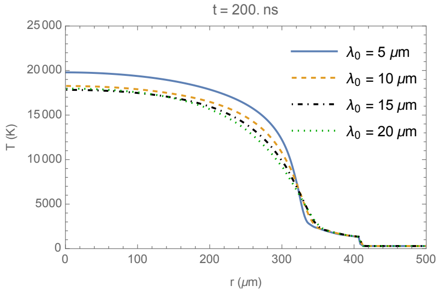


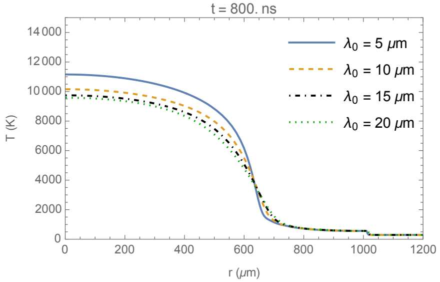

# Radiative MFP study, effects on temperature (on axis)

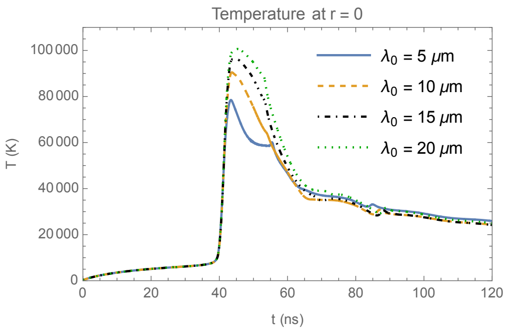


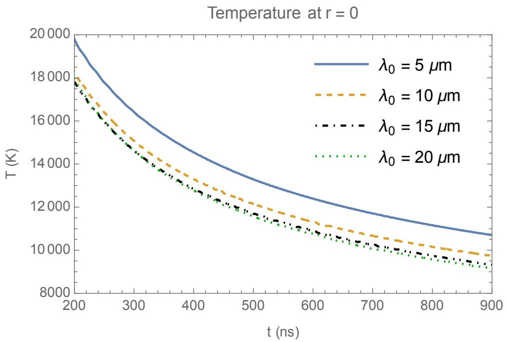


- Temperature on axis *higher* for larger $\lambda_0$ at earlier times, but *reversed* trend at later times
  - More effect cooling during later stages of discharge
  - Opposite behavior to density (consistent with pressure mostly independent of $\lambda_0$)
- Variation in peak temperature (on axis) of about 80,000 to 100,000 K.

# Model validation against CSM experiments

# Model comparison with circuit measurements of CSM spark gap experiments

- All data compared with here used atmospheric (low-humidity) air with rounded (spherical) electrodes
  - Taken by C. A. M. Schrama (2022-2023)
- Data from two types of apparatus:
  - Enclosed (gas-tight chamber) spark gap with $C = 100\ \mathrm{pF}$, $L \approx 150\ \mathrm{nH}$
  - Open air spark gap with $C = 700\ \mathrm{pF}$, $L \approx 1170\ \mathrm{nH}$
- Current measurements used CVR with $R_v = 0.0983\ \Omega$ unless noted otherwise
- Density from model compared with 2-color interferometry data for enclosed spark gap (100 pF)
- Transport parameters used as listed here:

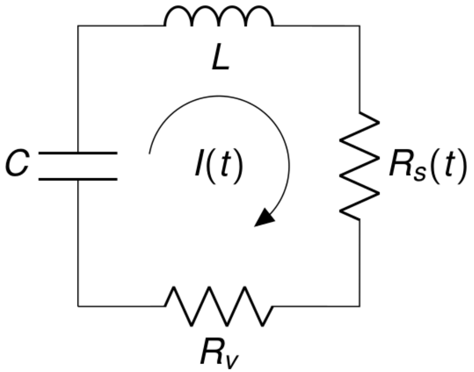


| $\log \Lambda$ | $\lambda_0\ (\mu\mathrm{m})$ | $\rho_0\ (\mathrm{kg/m^3})$ | $R_v\ (\Omega)$ | $\sigma_s(r, t=0)$ |
|---|---|---|---|---|
| 15 | 20 | 1.2 | 0.0983 | IC1 |

# 100 pF enclosed spark gap with air

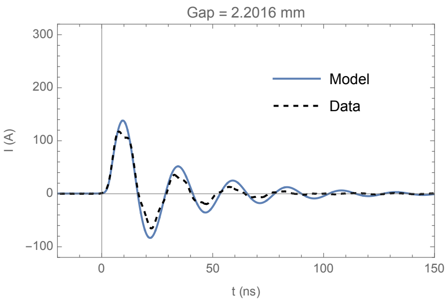


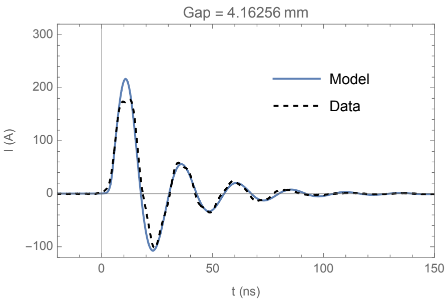


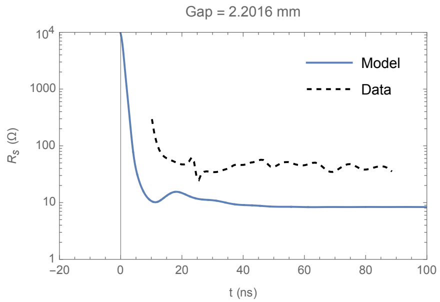


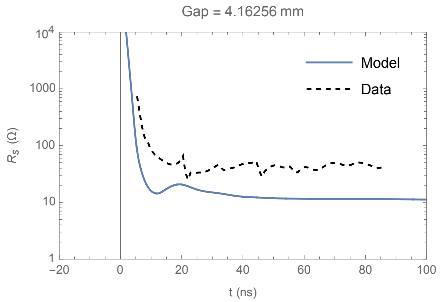


Current

Spark resistance

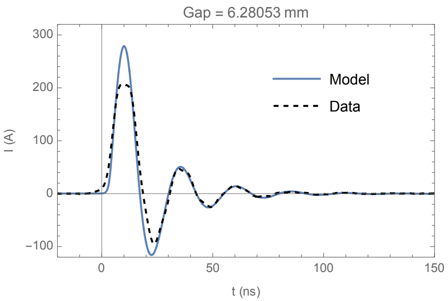


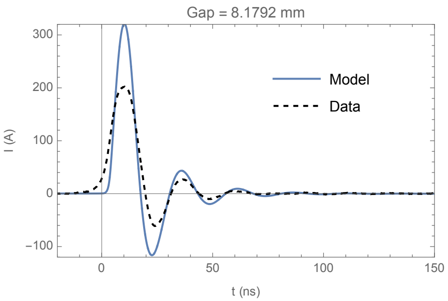


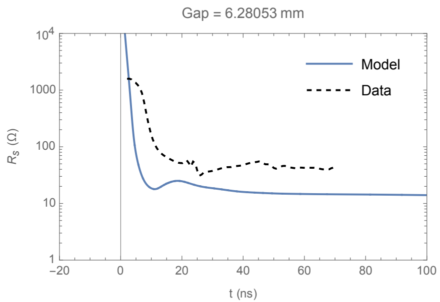


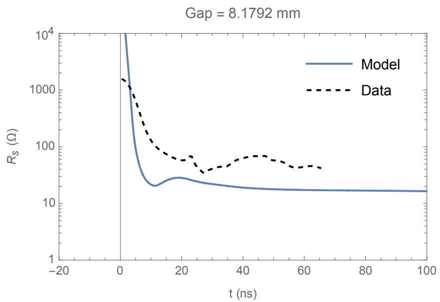


- Model peak current slightly higher
- Model $R_{s,\min}$ lower by factor of 2-3

Gap lengths and initial voltages

| $\ell$ (mm) | $\varphi_0$ (kV) | $\mathcal{E}_0 = \frac{1}{2}C\varphi_0^2$ (mJ) |
|---|---|---|
| 2.2016 | 7.73096 | 2.98838 |
| 4.16256 | 12.7712 | 8.15512 |
| 6.28053 | 17.3125 | 14.9862 |
| 8.1792 | 20.8629 | 21.763 |

Los Alamos NATIONAL LABORATORY

# 100 pF enclosed spark gap with air

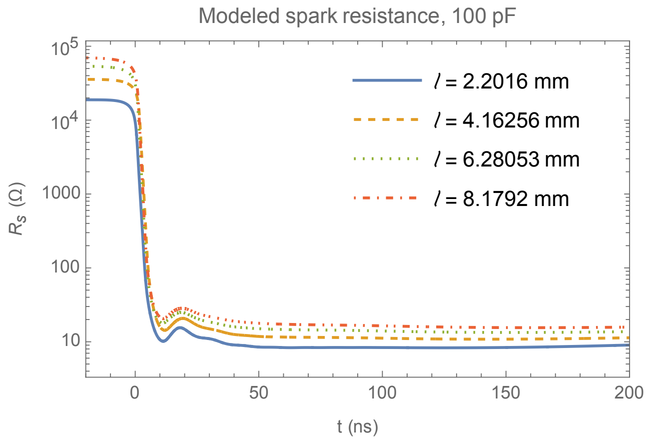


Gap lengths and initial voltages

| $\ell$ (mm) | $\varphi_0$ (kV) | $\mathcal{E}_0 = \frac{1}{2}C\varphi_0^2$ (mJ) |
|---|---|---|
| 2.2016 | 7.73096 | 2.98838 |
| 4.16256 | 12.7712 | 8.15512 |
| 6.28053 | 17.3125 | 14.9862 |
| 8.1792 | 20.8629 | 21.763 |

- Experimental data had $R_{s,\mathrm{min}} \approx 40\ \Omega$, independent of gap length $\ell$
- Model had $R_{s,\mathrm{min}} \approx 10 - 20\ \Omega$, increasing with gap length
- Note: model and experimental data on previous slide both time-shifted to have current start at $t \approx 0$

Los Alamos NATIONAL LABORATORY

# 700 pF open air spark gap (no additional resistance)

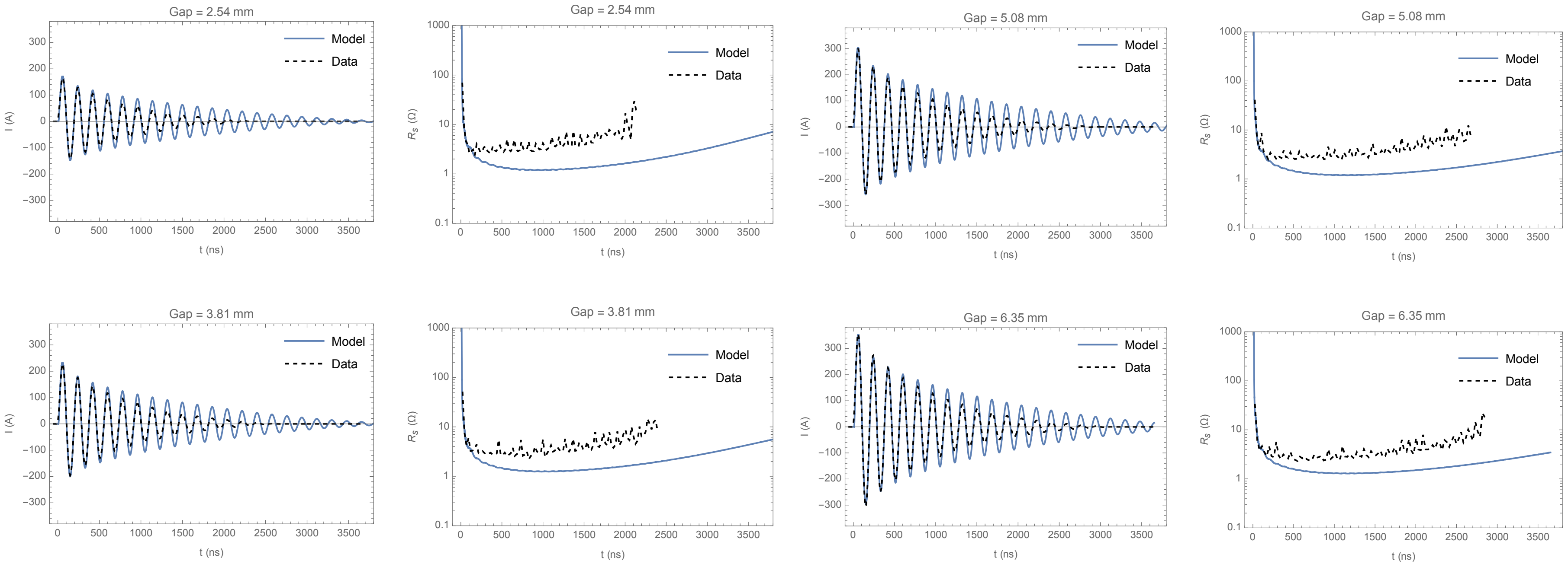


- Model $R_{s,\min} \approx 1 - 2\ \Omega$, while experiment had $R_{s,\min} \approx 2 - 3\ \Omega$
- Model takes longer to reach $R_{s,\min}$, but recovers at similar rate

Gap lengths and initial voltages

| $\ell$ (in) | $\ell$ (mm) | $\varphi_0$ (kV) | $\mathcal{E}_0 = \frac{1}{2}C\varphi_0^2$ (mJ) |
|---|---|---|---|
| 0.05 | 1.27 | 4.84903 | 8.22957 |
| 0.10 | 2.54 | 8.14846 | 23.2391 |
| 0.15 | 3.81 | 11.4153 | 45.6081 |
| 0.20 | 5.08 | 15.0776 | 79.5668 |
| 0.25 | 6.35 | 17.8054 | 110.961 |

Los Alamos NATIONAL LABORATORY

# 700 pF open air spark gap, additional series resistance

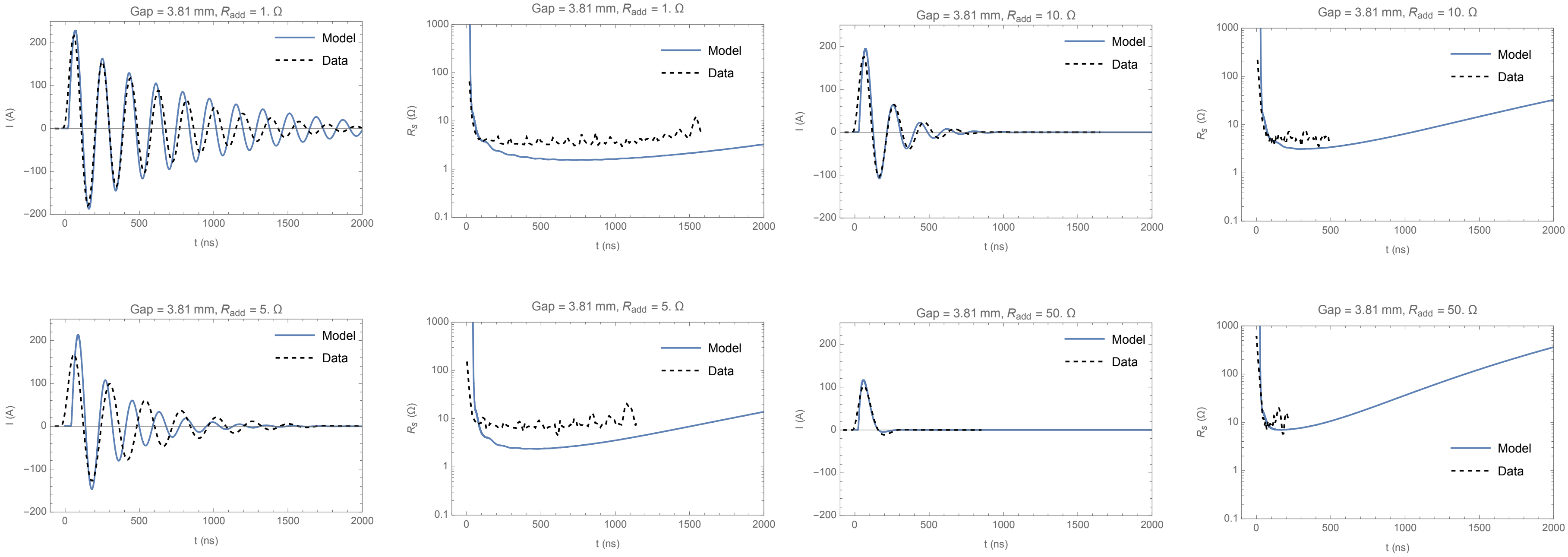


- Adding series resistance slightly changed inductance (experiment), strongest for $R_{\text{add}} = 5\ \Omega$
- Better agreement for $R_s$ as $R_{\text{add}}$ increased

| $R_{\text{add}}$ (Ω) | $\varphi_0$ (kV) | $\mathcal{E}_0 = \frac{1}{2}C\varphi_0^2$ (mJ) |
|---|---|---|
| 1 | 11.4319 | 45.7406 |
| 5 | 11.4146 | 45.6029 |
| 10 | 11.3667 | 45.2205 |
| 50 | 11.3128 | 44.7925 |
| 100 | 11.4125 | 45.5854 |

# 100 pF enclosed spark gap, interferometry setup

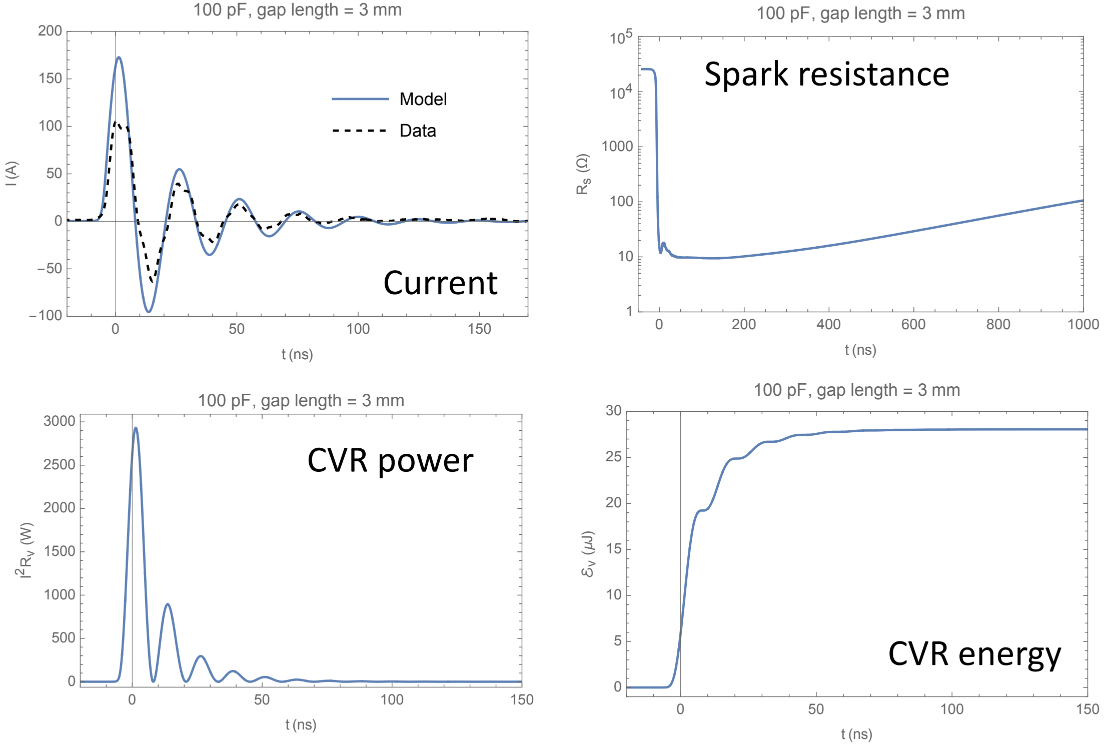


| $\ell$ (mm) | $\varphi_0$ (kV) | $\mathcal{E}_0 = \frac{1}{2}C\varphi_0^2$ (mJ) |
|---|---|---|
| 3.00 | 9.88419 | 4.88487 |

- $C = 100\ \mathrm{pF}$, $L \approx 150\ \mathrm{nH}$
- Similar trend for current as other 100 pF data
- ~3 kW max power to CVR, ~28 μJ energy dissipation
- Note experimental data **not** time-shifted, model shifted to match experiment's scope trigger timing

# Density of heavy species

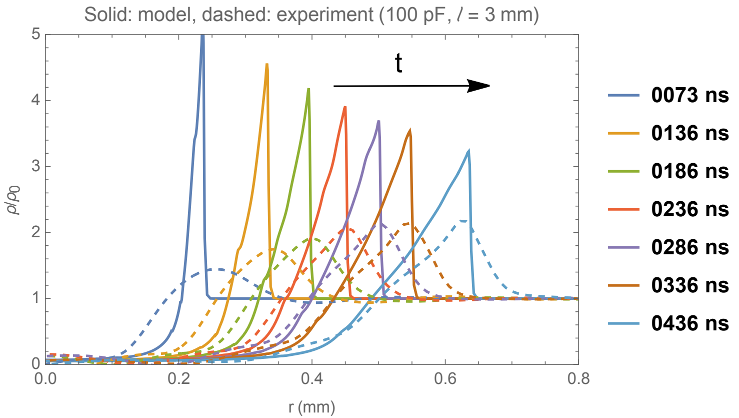


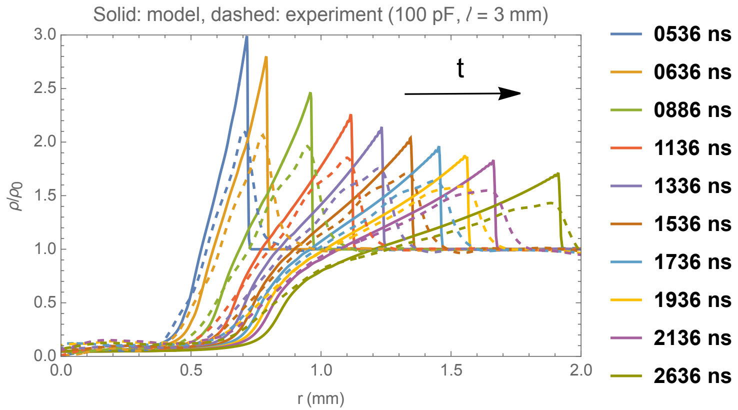


- Note: interferometry measures number density of heavy species normalized to ambient value
- Modeled $\rho/\rho_0$ matches well especially at later times and for rarefied region near axis of channel
- Resolution limits of interferometry setup seem to smear shock front

# Ionization fraction and density of electrons

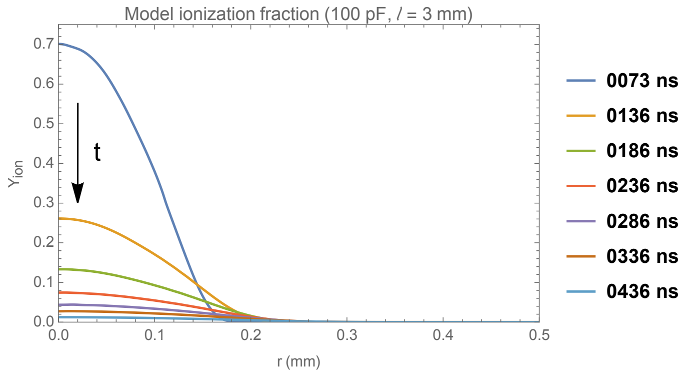


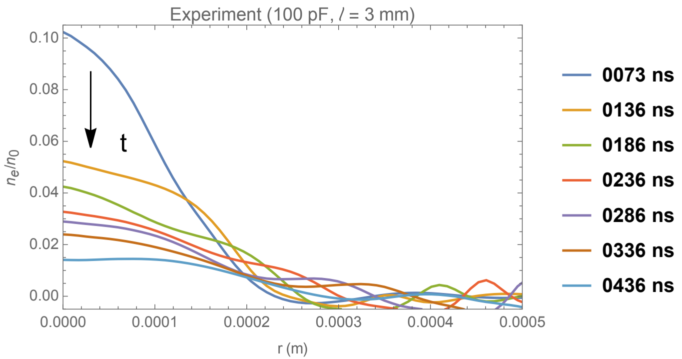


- Ionization fraction $\Upsilon_{\text{ion}}$ not directly comparable to measured $n_e/n_0$ (Note: $n_0$ is ambient density of particles (i.e. neutrals))
  - Still working out correct corresponding model variables, but all attempts so far still show similar trends to $\Upsilon_{\text{ion}}$
- Model ionization decays faster than data (but note noise floor on experiment)
- However, modeled ionized region has a similar size and profile to the data

# Summary, conclusions, and future work

# Summary, conclusions, and future work

- To model spark discharges, this work implemented, verified, and validated:
  - 1-D radial conservative Lagrangian hydrodynamic scheme (with heat conduction)
  - Eddington/P1 radiative transfer approximation, time-implicit scheme
  - RLC circuit solver, time-implicit scheme (adaptable to other circuit types)
- Novel analytic EOS fit for air up to temperatures of ~150,000 K
- Novel "seed" electron concept to initialize finite conductivity in spark without pre-heating the air in the channel, as typically used in spark modeling literature
- Reasonable, if conservative (from engineering viewpoint), agreement with experimental data for indirect (circuit) and direct (interferometry) measurements of spark
- Many potential avenues of **future work**:
  - Two-temperature hydrodynamics (requires two-temperature EOS development)
  - 2-D axisymmetric geometry for axial (z) variation, modeling dielectric electrodes
  - Kinetic equations for time-dependent charged species populations

# Acknowledgments


- Chip Durfee, David Flammer, Liam Pocher, Claudia Schrama, Sarah Hinnegan, Calvin Baylor, and other past/current members of the CSM physics ESD research team
  - CSM ptychography imaging team: Dan Adams, Jonathan Barolak
  - Fellow CSM physics grad students: Nick Materise, Paul Niyonkuru, Alan Philips, Taylor Wagner, and others
  - The faculty and staff of the CSM physics department
- Dan Borovina and Jonathan Mace at LANL for initiating and guiding the ESD research and characterization project
  - Travis Peery, Shane Fuller, and other staff members of W-10
  - The LANL Atomic Physics team (Eddy Timmermans, Dima Mozyrsky, James Colgan, Mark Zammit, and others) for atomic physics data and discussions about spark discharges
  - Jeff Leiding (T-1) for the Magpie tabular air EOS data
  - Tariq Aslam (T-1) for suggesting hydrodynamic methods and EOS fitting approaches
- My family: Bill, Terry, Kelly, Anne, and Neal
- The support of LANL, the DOE, and the NNSA for funding this effort

# Backup slides

# Noh shock reflection problem (cylindrical results)

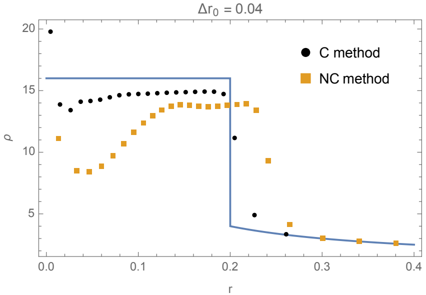


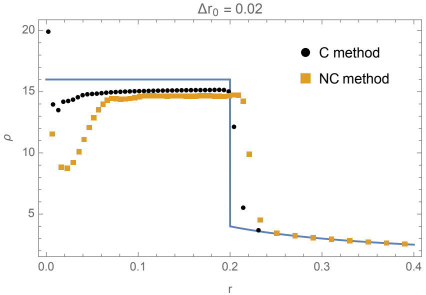


Density

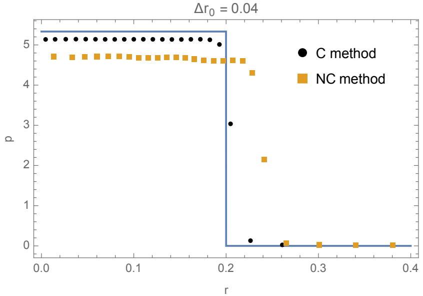


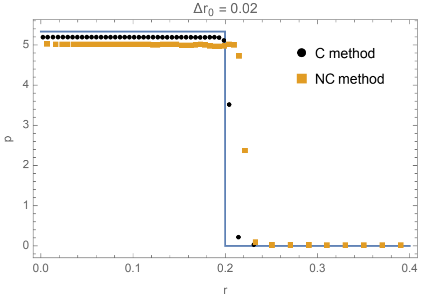


Pressure

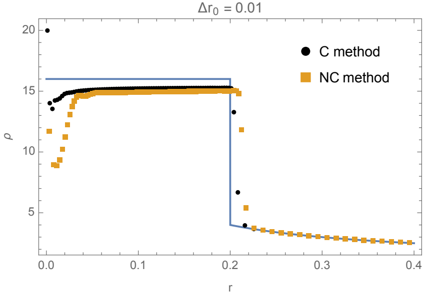


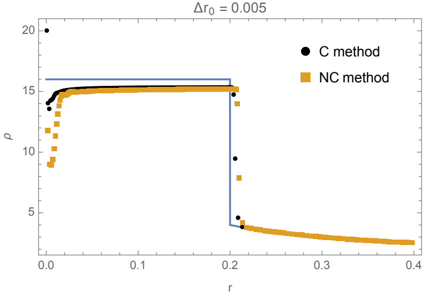


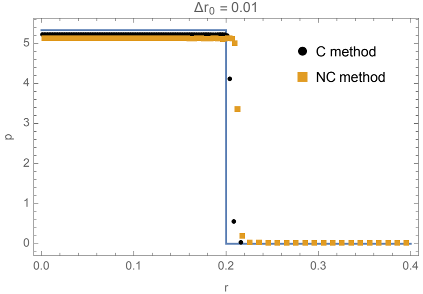


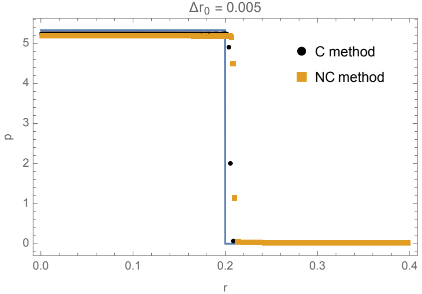


- Verified with ideal gas, $\gamma = 5/3$
- Much more difficult for Lagrangian methods than Sedov

Los Alamos NATIONAL LABORATORY

# Noh shock reflection problem (cylindrical results)

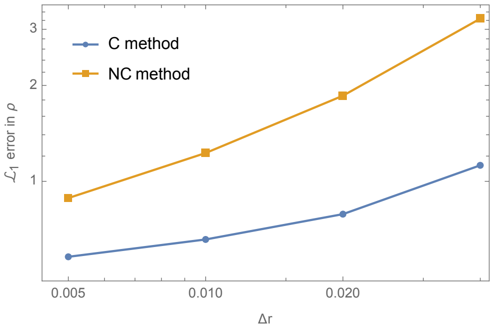


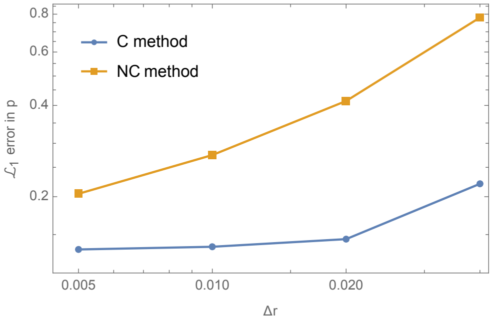


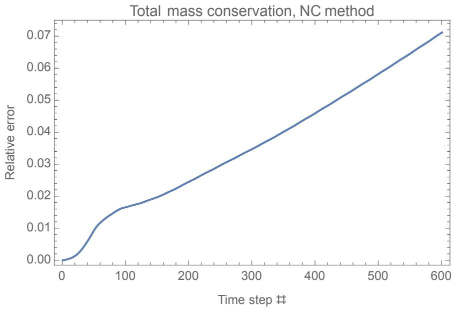


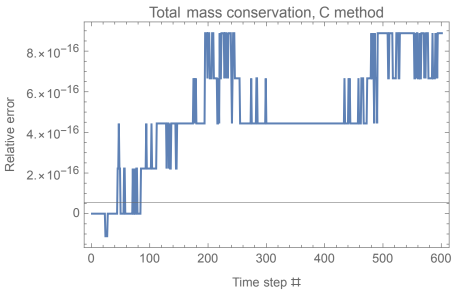


- $\mathcal{L}_1$ norm much below first order convergence
- “C” scheme still outperforms “NC” scheme, but both struggle with this particular problem

Los Alamos NATIONAL LABORATORY

# 100 pF enclosed spark gap interferometry (model vs experiment at individual times)

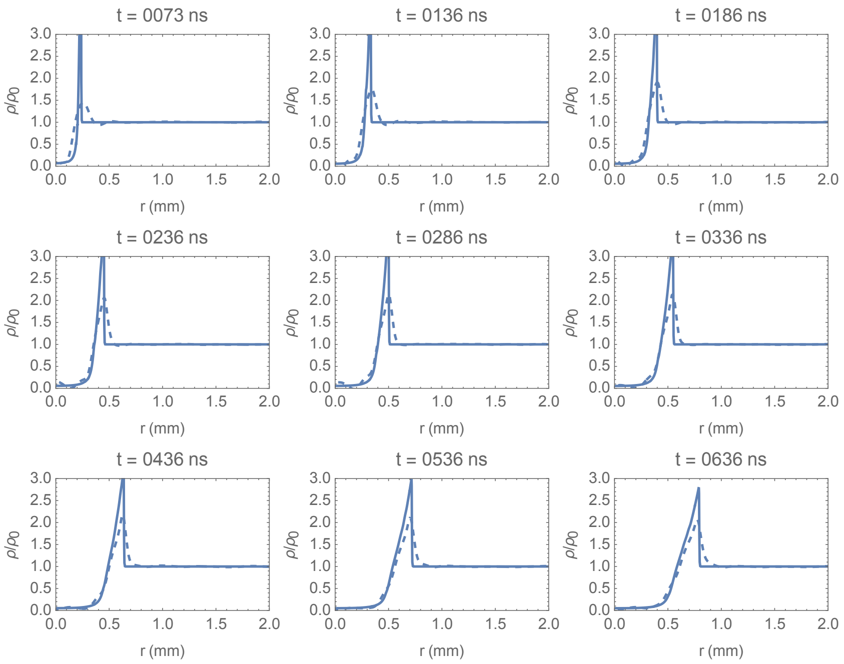


Density, model (solid) vs experiment (dashed)

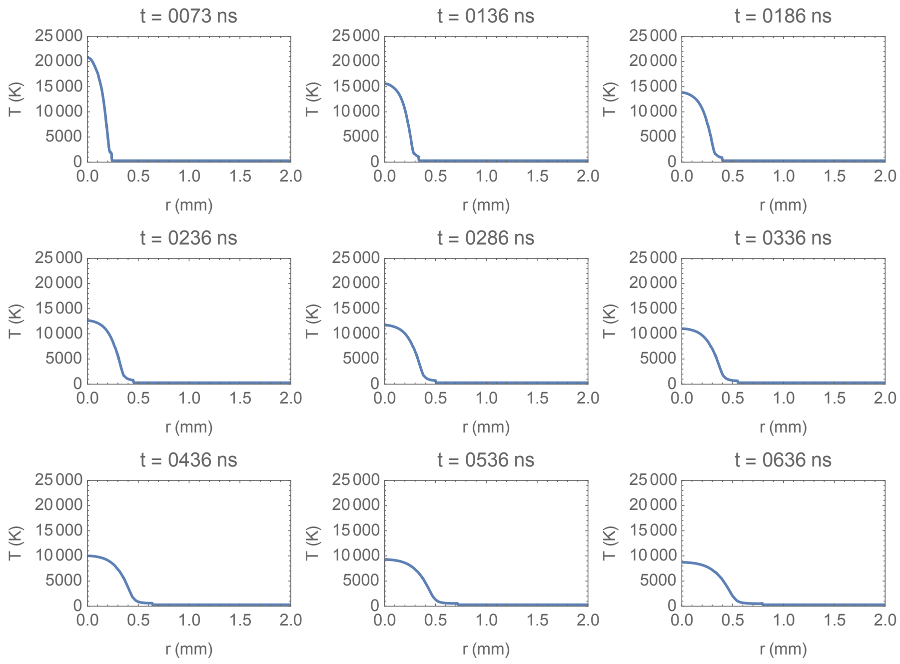


Temperature, model

# 100 pF enclosed spark gap interferometry (model vs experiment at individual times)

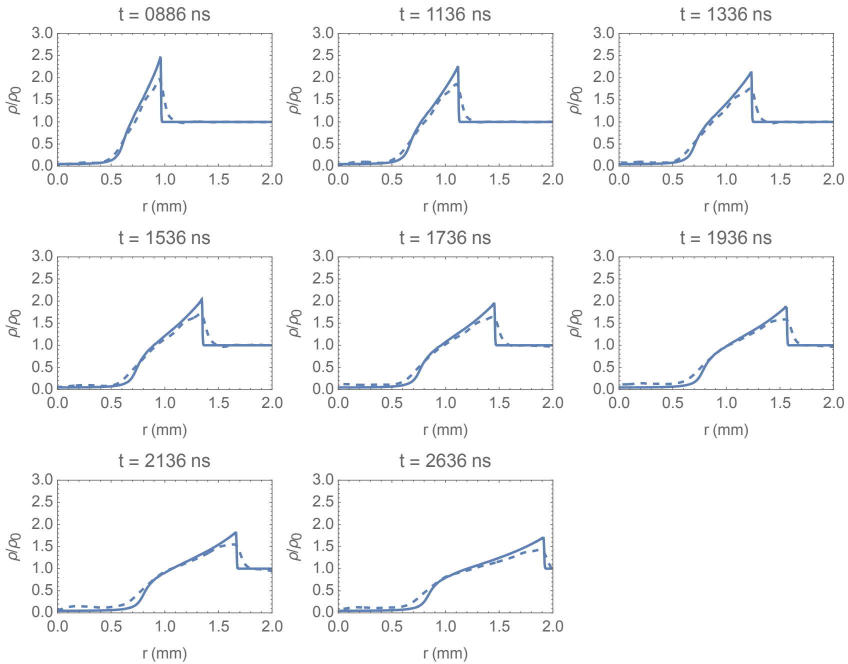


Density, model (solid) vs experiment (dashed)

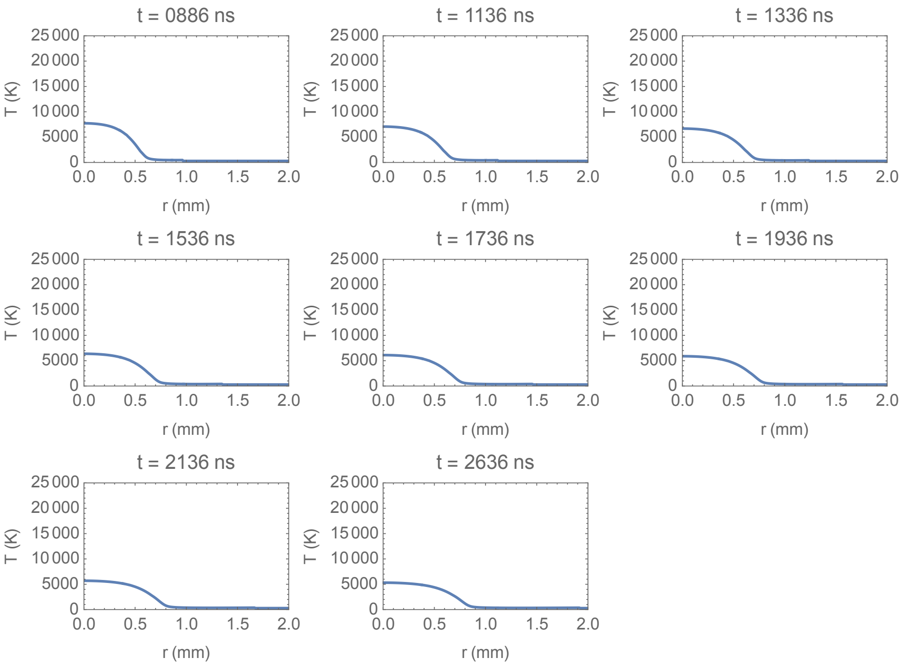


Temperature, model

# 100 pF enclosed spark gap interferometry (modeled temperature and energy density on axis of symmetry)

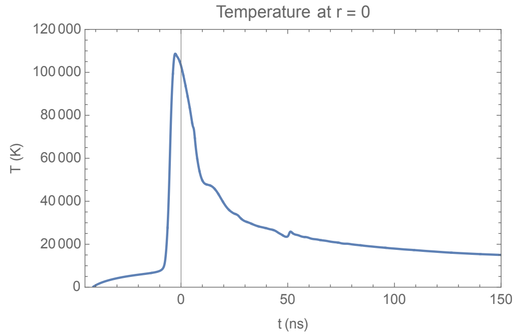


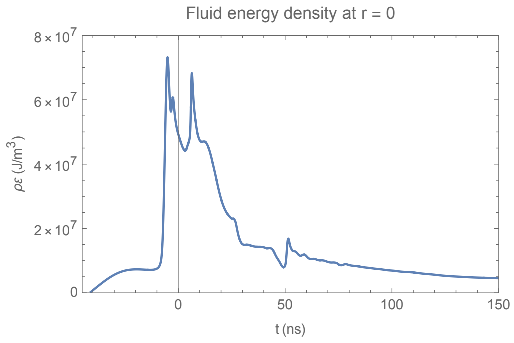


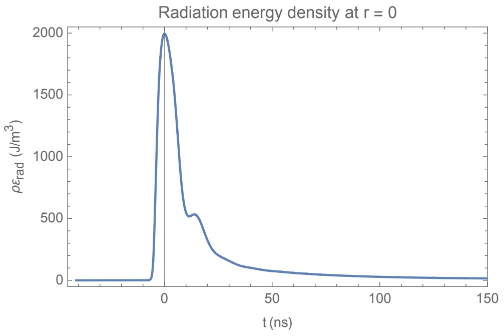


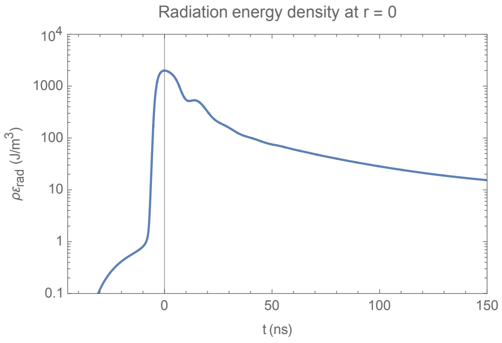


- Temperature only exceeds 50,000 K for a duration of ~20 ns
- Fluid energy density 4 orders of magnitude greater than radiation energy density (at peak values)
  - Necessary condition for weakly-coupled P1 approximation to radiative transport

# Another way of comparing model versus experimental interferometry data for electron population

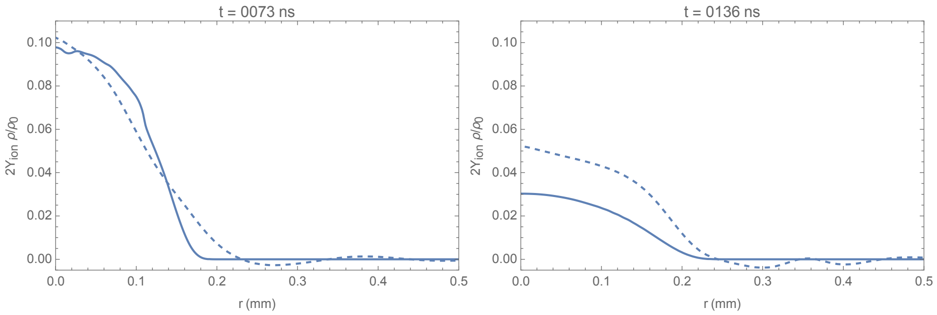


- Still decays much faster for model than experiment
- Noise floor for interferometry comes into play around 300—400 ns (overall density on axis becomes too low)

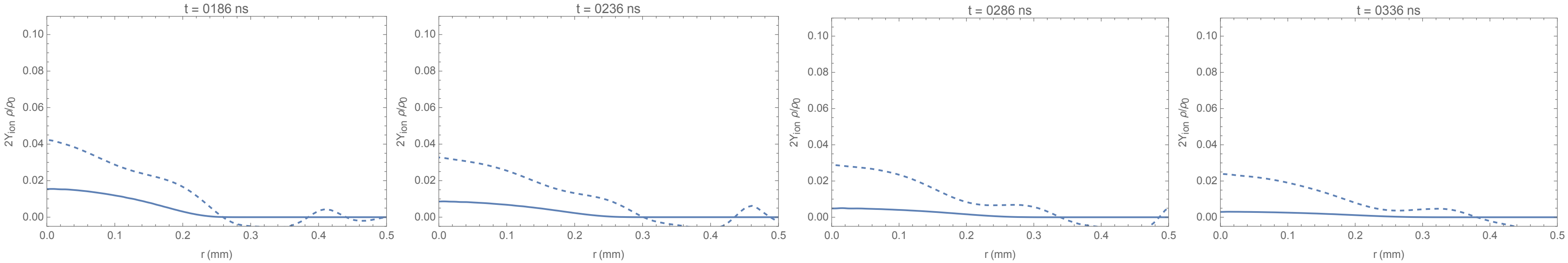


Los Alamos
NATIONAL LABORATORY